SAR DATA ANALYSIS ON FLOOD MAPPING USING PYTHON

A
MAJOR PROJECT REPORT

Submitted in the partial Fulfillment of the requirements for the award of the Degree of

BACHELOR OF TECHNOLOGY
IN
ELECTRONICS AND COMMUNICATION ENGINEERING

Submitted By

1. U.Vamsi Srinivas Rao	18R21A04H8
2. K.Kethan Mitra	18R21A04G7
3. D.Sarva Sree	18R21A04D2

UNDER THE GUIDANCE OF

Mr. P. Ramesh
(Assistant Professor)

MARRI LAXMAN REDDY GROUP OF INSTITUTIONS

MLR Institute of Technology

(Autonomous)

(Affiliated to JNTUH, Hyderabad)

Dundigal, Hyderabad-500043

2018-2022

MARRI LAXMAN REDDY GROUP OF INSTITUTIONS

MLR Institute of Technology

(Autonomous)

(Affiliated to JNTUH, Hyderabad)

Dundigal, Hyderabad-500043

MARRI LAXMAN REDDY GROUP OF INSTITUTIONS

DEPARTMENT OF ELECTRONICS AND COMMUNICATION ENGINEERING

CERTIFICATE

This is to certify that the project *entitled* ***"SAR data analysis on flood mapping using python"*** *is the bonafied work done by, U.Vamsi Srinivas Rao- 18R21A04H8, K.Kethan Mitra -18R21A04G7, D.Sarva Sree -18R21A04D2,* in partial fulfillment of the requirement for the award of the degree of B.Tech in Electronics and Communication Engineering, during the academic year 2021-22.

Internal Guide
(Mr. P. Ramesh)

Head of the Department
(Dr. S.V.S Prasad)

External Examiner

ACKNOWLEDGEMENT

We express our profound thanks to the management of **MLR Institute of Technology**, Dundigal, Hyderabad, for supporting us to complete this project.

We take immense pleasure in expressing our sincere thanks to **Dr.K.Srinivasa Rao**, Principal, MLR Institute of Technology, for his kind support and encouragement.

We are very much grateful to **Dr S.V.S Prasad**, Professor & Head of the Electronics and Communication Engineering Department, MLR Institute of Technology, for encouraging us with his valuable suggestions.

We are very much grateful to **Mr. P.Ramesh, Assistant Professor** for his unflinching cooperation throughout the project.

We would like to express our sincere thanks to the teaching and non teaching faculty members of ECE Dept., MLR Institute of Technology, who extended their help to us in making our project work successful.

Project associates:

U. Vamsi Srinivas Rao 18R21A04H8
K. Kethan Mitra 18R21A04G7
D. Sarva Sree 18R21A04D2

ABSTRACT

India is one of the most flood-prone countries in the world and one-eighth of the country's geographical area is subjected to floods. The flood extent mapping is critical to disaster management, humanitarian relief work and decision-making . Efficient monitoring and prediction of floods and risk management for a large river is quasi-impossible without the use of Earth Observation (EO) data from space. As a matter of fact, one of the most important problems associated with flood monitoring is the difficulty to determine the extent of the flood area as even a dense network of observations cannot provide such information. The flood extent information is used for damage assessment and risk management, and benefits to rescuers during flooding; it is also very important for calibration and validation of hydraulic models to reconstruct what happened during the flood and determine what caused the water to go where it did.

So basically what we are doing in this project is we take a level 1sar image, we process it using different steps, we will plot all the water bodies in that image ,after that we will mask the known water bodies leaving with the visual of extra water bodies that are present in flood prone areas. And we will writhe the output image in geotiff file. With this we will get a overview idea of where the flood water already reached. Processing of sar data is useful in this case because normal optical satellite images will be hindered by clouds and is hard to map water bodies. But with SAR images we can observe the terrain even though there are many obstacles like clouds dust etc as it is Radar Tech unlike optical one.

TABLE OF CONTENTS

LIST OF FIGURES

CHAPTER-1

INTRODUCTION

1.1 Earth Observation

Earth observation missions are designed to continuously monitor the earth to monitor the environment, land surface, biosphere, solid Earth, atmosphere, and oceans. The first earth observing satellite (Sputnik- 1) was launched on October 4, 1957, by the Soviet Union [1]. Explorer-1 was the first American satellitelaunched by NASA on January 31, 1958 [2]. Indian Space Research Organization (ISRO) has launched many Earth-observing (EO) satellites since 1979, beginning with Bhaskara - I, as it was the first experimental remote sensing satellite built by ISRO [3]. Indian Remote Sensing Satellite (IRS-1A) was the first series of indigenous remote sensing satellites launched into orbit on March 15, 1988. As of today,ISRO has launched 30 (27 optical and 3 Radar) Earth Observation missions and also has the largest constellation of remote sensing satellites in operation [4]–[5]. Earth-observing satellites are mainly used for remote sensing purposes to monitor the earth continuously. Satellites with optical sensors were providing the data from the past three decades with limitations.

1.1.1 Microwave Remote Sensing

Remote Sensing is the art and science of acquiring information without any physical contact. EO missions use remote sensing techniques to capture and analyze the Earth's terrain continuously using Space-borne satellites. Remote Sensing is categorized into two parts: 1) Passive Remote Sensing, 2) Active Remote Sensing. Passive Remote Sensing uses the sun as the source of illumination and capturesthe return radiance response onboard. Active remote sensing uses its source of illumination without depending on the sun as a source of energy [6]. Passive remote sensing uses optical cameras and scannersfor imaging. Common passive sensors are Landsat-7, Geo Eye, Quick Bird, Ikonos, and IRS. Active remote sensing uses RADAR, SONAR, and LIDAR to capture the earth's surface. Alos palsar-2, Radarsat-2, Sentinel-1 are the commonly used Active sensors. Remote sensing can be performed on various platforms such as spacecraft, aircraft. In remote sensing, the resolution depends on the sensor's height; the higher the height lower the resolution [7].

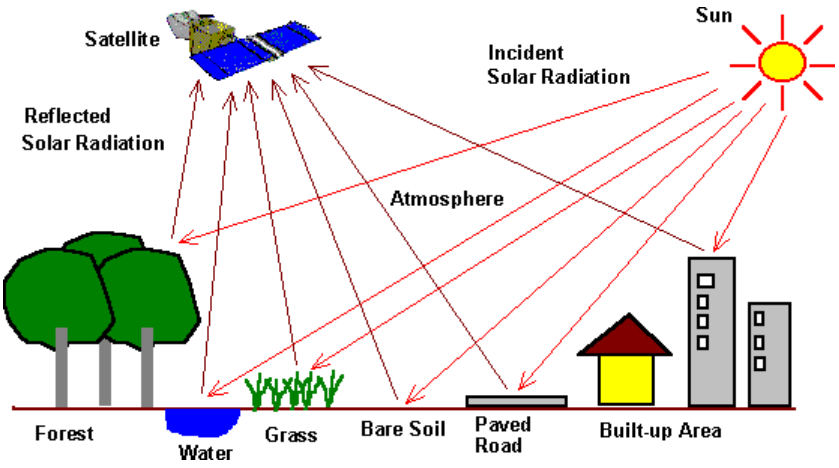

Fig .1.1 Illustration of Optical Remote Sensing

In Optical remote sensing, the sun is the source of illumination. The sensors on the satellite make useof visible, near-infrared, and short wave infrared rays to form the images of the earth's surface by detectingthe reflected solar radiation from the targets (water, forest, grass, building, and bare soil) on the ground as shown in Fig 1.1. The sensors mounted on the satellite can image only in daylight and in perfect weatherconditions with limitations.

In Microwave Remote sensing, sensors use the microwave region of the electromagnetic spectrum. The sensor in microwave remote sensing is called an antenna. RADAR is an acronym for Radio Detectionand Ranging. RADAR is a type of antenna which can transmit and receive the electromagnetic signal from the targets. RADAR uses the microwave region of the electromagnetic spectrum from P-band (0.3 GHz) to K_a-band (40 GHz) to transmit and receive, as shown in Figure 1.2. The Development of RADARtook place during World War II for navigation and target location. Imaging radars are operated in the range of 1mm to 1-meter wavelength, as longer wavelengths improve signal penetration through the atmosphere and clouds [9]. In the microwave, remote sensing resolution is independent of the sensor mounted altitude but dependent on the length of the antenna. The longer the antenna length, the greater the resolution, but practically it is difficult to deploy a longer antenna into space [7].

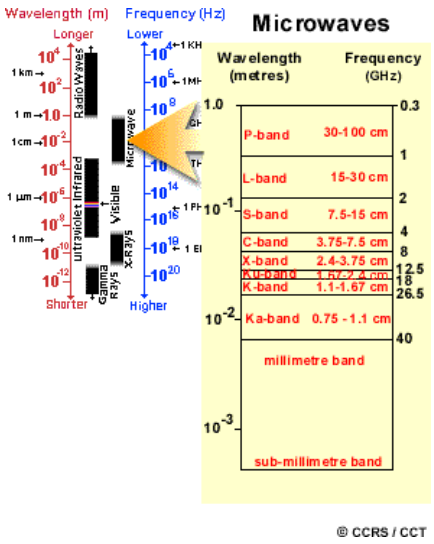

Fig 1.2 Electromagnetic spectrum © (CCRS)

1.1.2 Why Microwaves for Remote Sensing

Microwaves can penetrate through clouds and, to an extent, rain. Microwaves do not rely on sunlight as a source of illumination. These attributes allow sensing the earth's surface independently of the day and almost in all weather conditions [8]. Microwaves can penetrate through vegetation, soil, ice than optical waves. Longer microwave penetrates much better than shorter avelengths, as shown in Figure1.3, the most crucial reason for the use of microwaves is the information content available is different from visible and infrared regions of the electromagnetic spectrum.

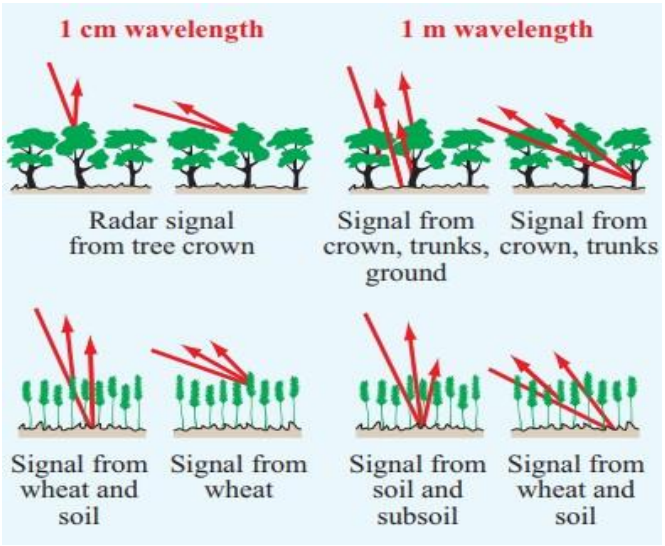

Fig 1.3 Radar signal penetration for different wavelengths

1.1.3 Advantages and disadvantages of Microwaves Remote Sensing over Optical Remote Sensing

Advantages	Disadvantages
Nearly all-weather capability	The Information content is different from Optical
Day or Night capability	Difficult to interpret the information
Penetration through vegetation Canopy	Speckle effects
Penetration through soil	Topographic effects
Minimal Atmospheric effects	
Sensitivity to dielectric properties of the Target	
Sensitivity to structure of the targets	
Unique Sensitivity to moisture content of the Target	
Unique Sensitivity towards the orientation of the target	

Table 1.1- Advantage and disadvantages of Microwave Remote sensing

1.2 Overview and History of Microwave Remote Sensing

P-band, L-band, S-band, C-band, and X-band are the frequently used microwave bands for imaging. Active microwave sensors are categorized into imaging and non-imaging sensors. Altimeters and scattermeters are the non-imaging sensors. Imaging Radar is operated in two platforms a) Airborne platform b)Space-borne platform. From these platforms, RADAR can be used in nadir looking, Side looking. Real Aperture Radar (RAR) is an example of nadir looking sensors. Side Looking Airborne Radar (SLAR) andSynthetic Aperture Radar (SAR) are examples of side-looking sensors.

1.2.1 Imaging Radar

James clerk Maxwell (1831-1879) provided the fundamental mathematical descriptions of the magnetic and electric fields associated with electromagnetic radiation. In the year 1886, Hertz demonstrated the transmission of Radio microwaves and reflections from various objects. Hertz also studied the interaction of radio waves with a metallic surface. Based on the fundamental physics

principlesdiscovered by Maxwell and Hertz, M. Marconi (1874 -1937) constructed an antenna that transmitted andreceived radio signals. A.H Taylor and L.C investigated RADAR. Young in the year 1922. RADAR wasinitially used to detect targets such as ships and aircraft, both friendly and enemy. In 1935, Young and Taylor and Sir Robert Watson-Watt independently combined antenna transmitter and receiver in the sameinstrument. These advancements in RADAR laid the ground-work for the development of RADAR in World War [9].

The imaging radar's origin came from the first airborne scanning radar system, H2S, developed by theRoyal Air force Bomber Command during World War II. It helped to identify the targets on the ground surface in all weather and even through clouds. The critical development was to use high frequencies longantennas capable of producing narrow beams projecting sideways from the aircraft. This resulted in extensive coverage by scanning along the flight path known as Side Looking Airborne Radar (SLAR). In1952, the critical development of the technique "Doppler beam sharpening" took place in the Goodyear Aircraft Corporation by Carl Wiley. In the mid-1960s, there are two types of SLAR: Real Aperture Radarand Synthetic Aperture Radar.

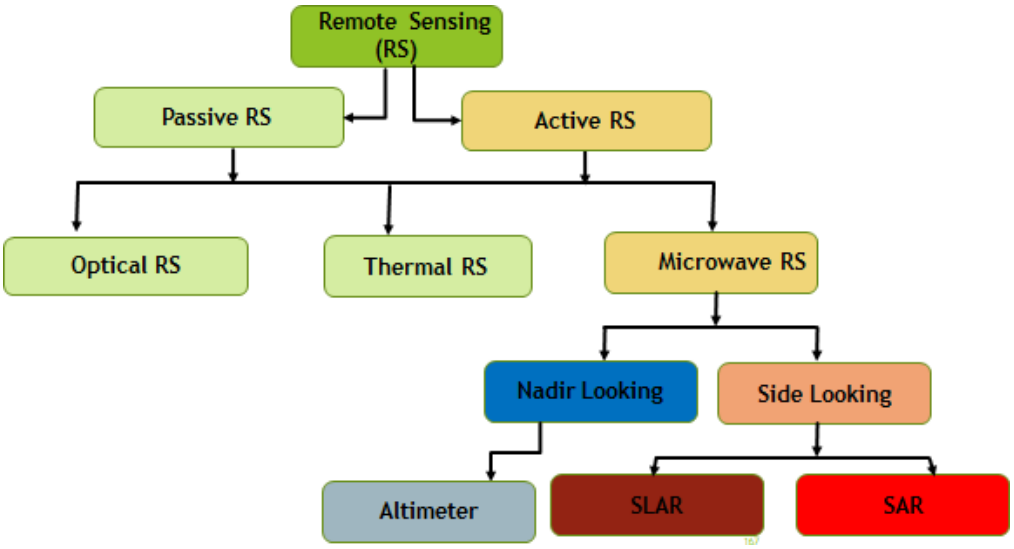

Fig 1.4 Family of Remote Sensing

1.2.2 Radar Image construction

The Radar instrument is placed on a spacecraft/aircraft and pointing the antenna sideways, i.e. tilting the antenna with a viewing angle as shown in Fig 1.5. The basic idea was to introduce to make spatial measurement of the backscattered signal from the target using a scatterometer. The distance on the groundis related to the time delay of the backscatter. Thus the construction of a two dimensional image is generated by utilizing the motion of the radar antenna to scan the earth surface along with the motion of the sensor.

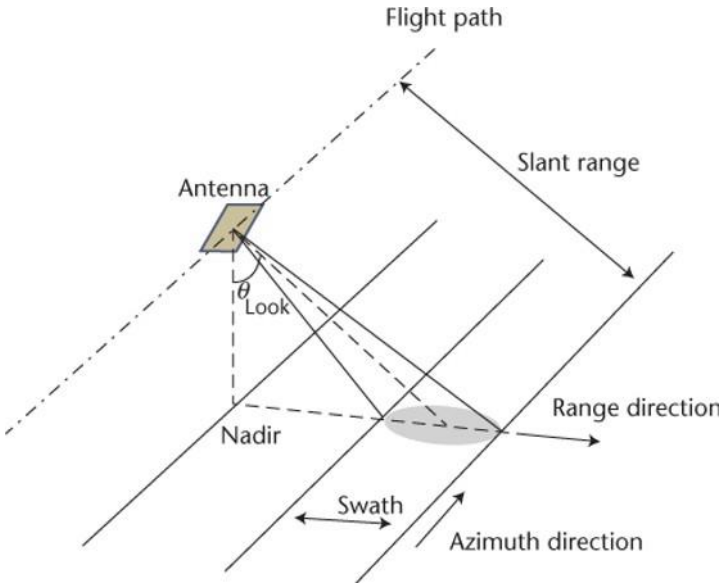

Fig 1.5 Radar Imaging Geometry © NASA

Azimuth Direction: The direction in which Flight is travelling.

Near Range: Minimum distance between target and antenna.

Far Range: Maximum distance between target and antenna.

Range Direction: Antenna beam direction from near range to far range.

Nadir: Perpendicular direction to the flight path

Swath: Distance between near range and far range.

Incidence angle: Angle to nadir.

Radars are classified depending upon their look direction

- Nadir Looking
- Side Looking

In Nadir looking, the antenna is placed perpendicular to the flight path, as the footprint is circular the range between near range and far range will be the same. But in side looking, the antenna is tilted towardsthe flight direction shown in Figure 1.6.

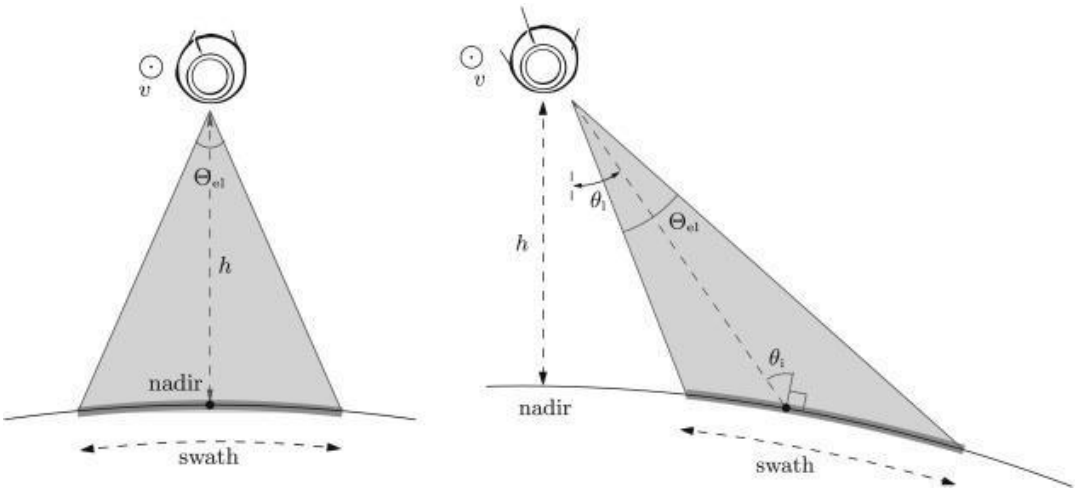

Fig 1.6 Nadir looking Radar and Side looking Radar

1.3 Synthetic Aperture Radar (SAR)

Synthetic aperture radar (SAR) is one of the most advanced engineering inventions in the twentieth century. SAR is a powerful remote sensing tool. The idea of SAR was initially mentioned in a Good yearAircraft report by Carl.A.Wiley in the year 1951 and was put into operation in early 1952 [10]. A SAR isan active sensor that first transmits a microwave signal and returns the backscattered signal from the earth's surface. In general, the larger the antenna's size, the unique information can be obtained by the SAR scientist. The more information, the better the image resolution. The space-borne or the airborne platform should deploy the larger antenna (10 m) to obtain better resolution. But, practically deploying such a larger antenna is infeasible. The scientist, therefore, used the motion of the spacecraft, along withthe advanced signal processing techniques they simulated a larger antenna. Microwave imaging (Microwave Remote Sensing) 's motivation came from its unique features such as weather independent, day and night imaging capability, geometric resolution independent of the distance, penetration of radar waves through atmosphere, clouds, vegetation, and even though the soil. SEASAT was the first-ever civilian spaceborne radar remote sensing system launched by NASA/JPL in 1978. Later, few SAR missions such as ERS-1, 2 from Europe, JERS-1 from Japan, and Radarsat-1 from Canada were launchedin the '90s and proved the potential of SAR Remote Sensing [11].

1.3.1 SAR Principle

SAR transmits a radar pulse towards the target and reflects back the pulse towards the transmitter, which depends on the type of scattering. Suppose the scatter, the surface is smooth. In that case, the incident energy will be reflected away from the sensor. If the scattering surface is

rough, then the incidentenergy will be diffused in all directions, and the sensor will receive only a part of the reflected power. The amount of backscattered energy depends on the properties of ground targets.

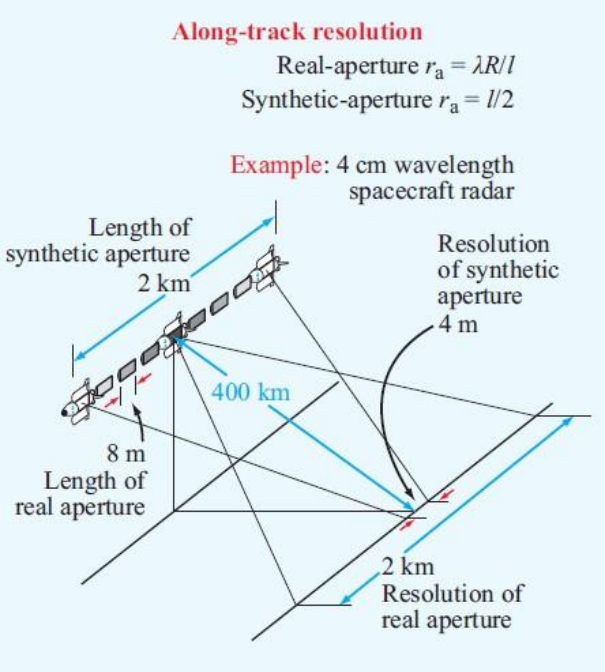

Fig. 1.7- Aperture Synthesis

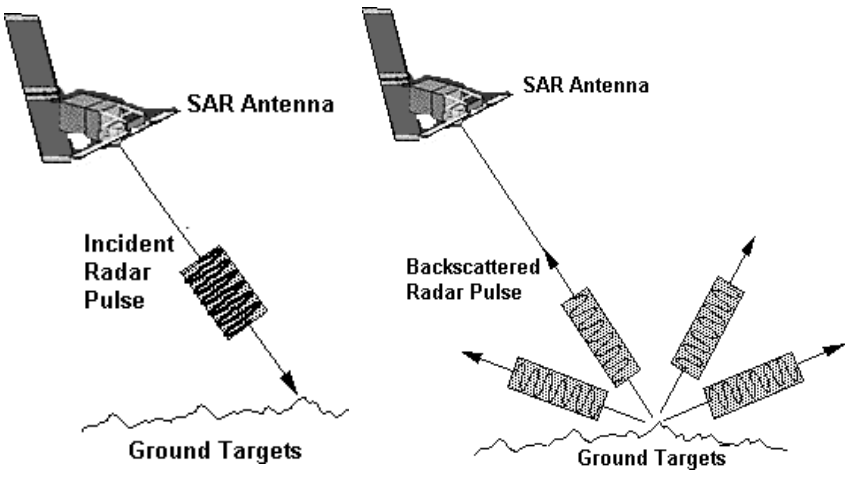

Fig 1.8 SAR principle

1.3.2 Resolution

The capability of a sensor to discriminate the smallest object on the ground. In SAR, there

are two types of resolution. 1) Range Resolution 2) Azimuth Resolution [12].

1.3.2.1 Range Resolution

To determine the spatial resolution at any point is a radar image, it is necessary to compute the resolution in two dimensions. Range and Azmimuth resolution. Radar is a ranging device that measures the distance to objects in the terrain using sending out and receiving pulses of active microwave energy. The range resolution in the across-track direction is proportional to the length of the microwave pulse. The shorter the pulse length, the finer the range resolution. Pulse length is a function of the speed of lightmultiplied by the duration of the transmissionτ . The length of time that the microwave energy is transmitted is measured in microseconds and typically ranges from 0.4 -1.0microseconds and translates into a pulse length ranging from 8 – 210m. The pulse length must travel to the target and back to the sensor. Therefore it is necessary to divide by 2 to measure the slant-rang resolution. And to scale it to ground-range, it is multiplied by the cosine of the depression angle (γ).

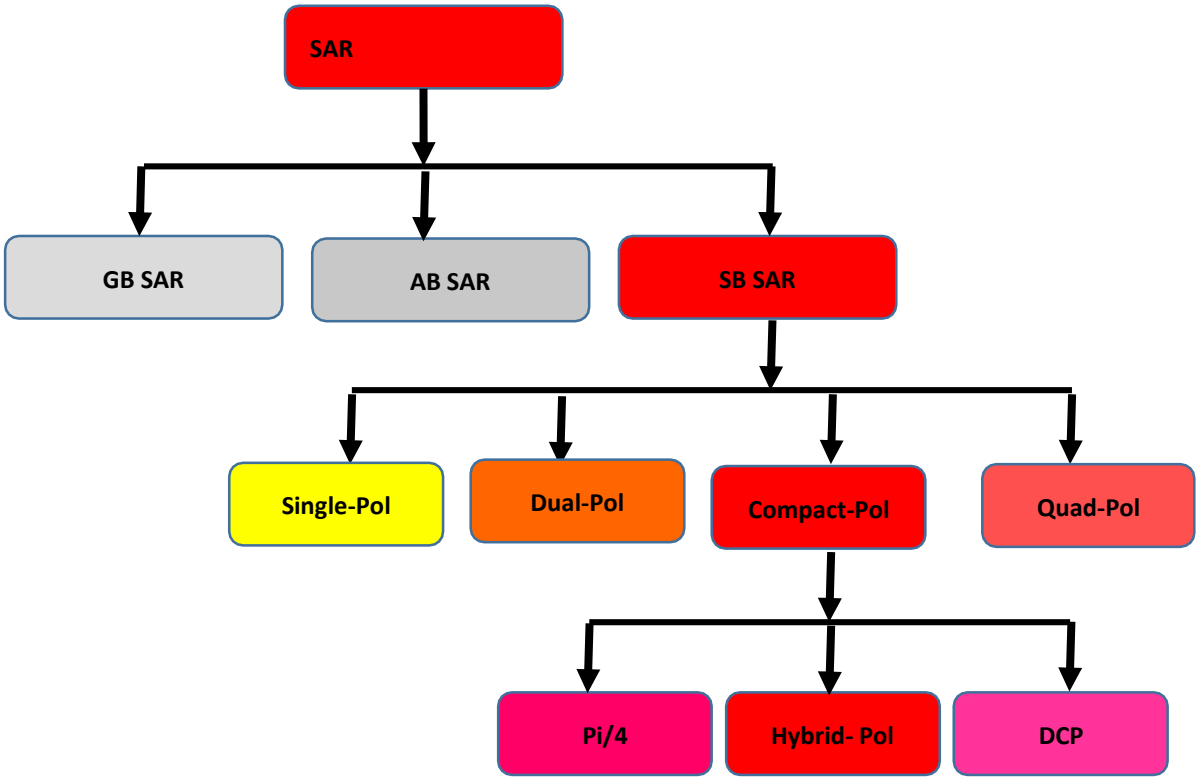

Fig 1.9 Family of Synthetic Aperture Radar

1.3.2.2 Azimuth Resolution Family of Synthetic Aperture Radar

Thus far, we have only identified the length in meters of an active microwave resolution element ata specific depression angle and pulse length in the range direction. To know both the resolution element'slength and width, we must also compute the width of the resolution element in the craft flying direction.Azimuth resolution (R_a) is determined by computing the terrain strip's width that is illuminated by the radar beam. Real aperture active microwave radars produce a lob-shaped beam.

1.4 Radar Polarimetry

It is a science of acquiring, processing, and analyzing the polarization state of an electromagnetic field.The polarization information contained in the backscattered wave from a given medium is related to its geometrical structure, reflectivity, shape, and orientation. There are four types of polarization 1) Single polarization, 2) Dual polarization, 3) Quad polarization 4) Compact polarization. In general, a single polsystem transmits and receives only one polarization, viz. horizontal (H) or vertical (V). Similarly, a dual-pol SAR transmits one polarization and receives the backscatter in a pair of orthogonal polarization viz. transmit (H) and receives (H, V) vice versa. In quad-pol SAR, two orthogonal polarizations H and V, arecoherently transmitted and received. In compact polarization, one linear polarization is transmitted, and two mutually coherent circular polarization is received. Complete polarimetric scattering information canbe obtained from the target from quad-pol SAR, and hence, better analysis and classification can be performed.

1.5 Scattering mechanism

They are four types of scattering mechanisms 1) Specular 2) Surface 3) Double bounce 4) Volumescattering.

Specular

When a radar signal is transmitted on flat terrain, the reflection angle is the same as the incidence angle; it is called specular reflection. These areas in the radar image appear very dark, e.g., smooth waterbody or tarmac.

Surface scattering

When a radar signal hits on a rough surface, some energy will be backscattered to the sensor. Example:vegetation, bare soil.

Double Bounce

When the radar pulse hits to smooth surface that is perpendicular to each other, the returned signal willbe strong and appears brighter in a SAR image. Example: Buildings and manmade structures.

Volume Scattering

When a man's radar pulse hits a three-dimensional body, the energy gets reflected multiple times in multiple directions. Examples are dense snow, forests.

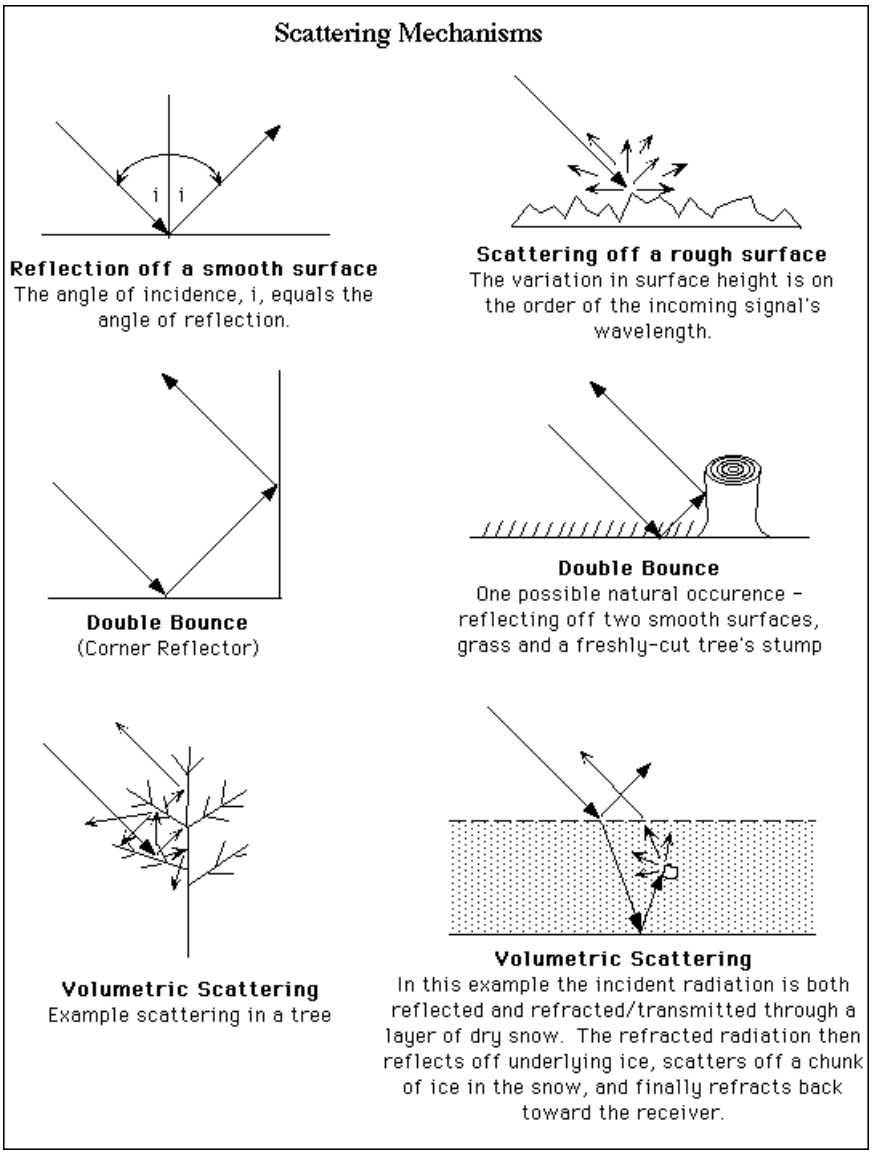

Fig 1.10 Scattering Mechanism © esa

1.6 Motivation

Earth Observation (EO) Missions are meant for continuous monitoring, and thus the SAR systemsrequire a huge amount of storage, higher transmission power, and larger swath width. SAR systems can image the Earth during rainy seasons and in the absence of sunlight, which is an advantage over traditional optical imaging systems. Therefore the data can be well utilized in disaster management. Generally, dual-pol SAR and quad-pol SAR are used for EO Missions. The dual-pol SAR cannot give more information than the quad-pol SAR, and the quad-pol SAR consumes a huge amount of energy with less swath widthand complex architecture. Compact polarimetry offers a tradeoff with fully polarimetric systems in terms of swath width, power, architecture, budget, and information content [13]. Compact polarimetry (Hybrid-pol) 's main difference from fully polarimetric systems is transmitting a circularly polarized signal towards the target and receiving linearly polarized returns [14]. While transmitting a circular component, ionosphere interaction will be reduced. RISAT-1 was the first EO mission built on Hybrid-poli

A rchitecture; therefore, original Hybrid-pol RISAT-1 data was used in this study [15]. It was compared to dual-pol and quad-pol data in the literature to explore the performance of simulated Compact-Pol data.All the studies so far performed on Hybrid-pol were simulated from quad-pol data [16]. This motivated us to investigate the performance of original Hybrid-pol data over dual-pol and quad-pol data. In the literature, a Comparison of Dual-pol and Hybrid-pol has been made using the data from different missions. The availability of Dual-pol and Hybrid-pol data from the same RISAT-1 mission with the exact resolution made us work on this topic. To compare the penetration capability, Alos palsar-2 (L- band) data and RISAT-1 (C-band) data have opted on the standard test site Sanfransico city.

Parameter	Launch date	Country	Wavelength,cm	Incident Angle	Polarization	Azimuth resolution	Range resolution	Swath width, km	Altitudekm
SEASAT	June 26, 1978	USA	L-(23.5)	[23^0]	HH	25	25	100	800
SIR-A	Nov 12, 1981	USA	L-(23.5)	[50^0]	HH	40	40	50	260
SIR-B	Oct 5, 1984	USA	L-(23.5)	[15^0-64]	HH	17-58	25	10-60	225 and 350
SIR-C/X-SIR	April 1994 Oct 1994	USA	X-(3.0) C-(5.8) L-(23.5)	[15^0-55^0]	HH, HV, VV,VH	30	10-30	15-90	225
ALMAZ-1	March 31, 1991	Soviet Union	S-(9.6)	[30^0-60^0]	HH	15	15-30	20-45	300
ERS-1,2	1991 1995	Europe	C-(5.6)	[23^0]	VV	30	26	100	785
JERS-1	Feb 11, 1992	Japan	L-(23.5)	[39^0]	HH	18	18	75	568
RADARSAT-1	November 1995	Canada	C-(5.6)	[10^0-60^0]	HH	8-100	8-100	50-500	798
ALOS PALSAR-2	May 2014	Japan	L-(22.9)	[8-70^0]	HH, HV, VV,VH	4.3	5.1	70km	691
RADARSAT-2	Dec 2007	Canada	C-(5.6)	[20-45^0]	HH, HV, VV,VH	3-80	1-100	18-500	798
RISAT-1	April 2012	India	C-(5.6)	[26.35^0]	RH, RV HH-HV	2.34	3.33		540

Table 1.2 Earth Observing (EO) SAR Missions

1.7 Literature Survery

This chapter presents a detailed literature survey on the Speckle filtering, the target decompositiontheorems and classification algorithms, compact polarimetry with existing state-of-art methods for processing and analyzing SAR images. We also discuss the literature around partial polarimetry. The author has collected ten base research articles

The concept of dual partial polarimetric mode was proposed by Je Souyris et al., the authors have assessed the performance of SAR compact Polarimetry architectures based on mixed basis measurement,i.e., transmitting polarization is either circular or oriented at an angle of 45°, and the receiver is at horizontal or vertical polarization. The performance is assessed in two folds: the first is concerned aboutthe information content preserved with comparing to FP SAR, and the second is to address the space implementation complexity in terms of swath width, power budget, calibration, and ionospheric effects. Because of the mismatch between transmitter and receiver bias, the power budget is deteriorated by a factor of 3dB [17].

Raney was the first person to build the Hybrid-Polarity SAR architecture on a space-borne

platform. In this, SAR transmits only one circular polarization and receives two mutually orthogonal linear polarizations. The author has introduced the m-delta decomposition technique in this paper. This paper's objective is full characterization and exploitation of backscattered response with a monostatic radar that transmits in one polarization is invariant to geometrical orientations in the scene. The Stokes parameters require measuring the relative phase, and the amplitudes of the received backscattered signal. The Hybrid-pol architecture minimizes sensitivity to relative errors, crosstalk, and optimizes relative phase and amplitude calibration. This architecture requires less RF hardware, less weight with fewer losses. The Hybrid-pol architecture systems will be an alternative for Earth Observations missions and a prime architecture for extraterrestrial missions. The study has demonstrated that hybrid-pol systems provide double swath width and less transmission power with simple architecture over quad-pol systems [13].

Michael E Nord, Thomas l, Ainsworth et al., (2009), the authors have compared the three compactpolarimetric modes. The authors have studied different transmit/receive configuration to determine which configuration allows for superior construction of full polarimetric data. The authors have noted that DCPand CLTR modes are related via bias change on the received signal. The authors have opted for L-band E-SAR data and simulated compact polarimetric modes. The single linear transmit will not excite returns from linear oriented structures, causing loss of polarimetric information. While transmitting a circular component misses some helical structure, which is less compared to a linear structure [18].

T.L Ainsworth, J.P.Kelly, J.S.Lee (2009), et al. Presented a study of the polarimetric information content of dual-pol imaging modes and dual-pol imaging extended by polarimetric scattering models. The authors have compared with Wishart classification on both partial polarimetric and full quad-pol datasets.In this study, NASA/JPL AIRSAR L-band airborne SAR data was used for the Flevoland region and L band E-SAR imagery of Oberpfaffenhofen. The authors have concluded that quad-pol data gave the mostaccurate results while performing Wishart classification and dual-pol data gave the most unsatisfactory results. The compact-pol data and pseudo-quad-pol data are the intermediates between dual-pol and quad-pol data. From the results on the Flevoland image, quad-pol data gave 81.8% accuracy, dual-pol data gave59.1% accuracy, compact-pol (Pi/4) data gave 80.9%, CLTR mode gave 81.8% accuracy, Pseudo quad- pol data (Pi/4) and CLTR gave 80.1%, and 73.5% accuracy respectively. From the results on Oberpfaffenhofen image, quad-pol data gave 97.5% accuracy, dual-pol data gave 96.1% accuracy, compact-pol (Pi/4) data gave 97.3%, CLTR mode gave 96.8% accuracy, Pseudo quad-pol data (Pi/4) and CLTR gave 97.2% and 95.1% accuracy respectively. The Hybrid dual-pol modes (Pi/4

and CLTR) not always perform better for image classification than standard linear dual-pol transmission [19].

A SAR system with Compact-pol architecture transmits a circular component and receives two mutually orthogonal coherent linear components, which is one manifestation of Compact polarimetry. The authors have utilized Radarsat-2 full polarimetric data to simulate Compact polarimetry. A researchteam composed of various departments of the Government of Canada evaluated compact- pol mode for various applications. Besides, the study has demonstrated the potential of Compact-pol for ship detection,soil moisture estimation, crop identification, and sea ice classification. The Compact-pol system provideda wider swath than a quad-pol system with simple architecture [20].

Rajib Kumar Panigrahi & Amit Kumar Mishra have compared hybrid-pol data with quad-pol schemes on the airborne GTRI dataset. This paper describes the benefits of using a hybrid-pol scheme. The comparison was made based on the information content, and it was concluded that the information of hybrid-pol is found to be comparable to that of the quad-pol airborne SAR system. However, hybrid- pol is the optimum choice when there is a requirement of wide swath cover, low transmission power [16].

Rajib Kumar Panigrahi & Amit Kumar Mishra have presented a comparison of Hybrid-pol and quad pol synthetic Aperture data (SAR) data for information content. First, the Hybrid-pol data was converted to pseudo quad pol data using compact polarimetric scattering models. The scattering mechanism was evaluated using Freeman and Durden decomposition techniques. In this study, NASA/JPL AIRSAR L-band airborne SAR data was used for the Flevoland region. The authors have evaluated and compared the scattering contribution for clusters of the pixels in SAR images. The authorshave concluded that the information content in pseudo quad pol is found to be comparable to quad pol data. Hybrid-pol data is the optimum choice when wider swath coverage and average transmitted power are the constraints [21].

Haldar, D., Das, A., Mohan, S., Pal, O., Hooda, R.S., and Chakraborty, M have evaluated L-band SAR data different polarization combinations, i.e., linear, circular, and Hybrid-polarimetric modes. The authors have opted for Alos-palsar full polarimetric data and simulated pi/4 mode and circular mode. Theauthors performed supervised classification using the maximum likelihood classifier on various polarimetric combinations. It has been observed linear full polarimetric mode gave an OA of (92%) followed by circular –full (89%), dual-circular (87%), hybrid-pol (7-75%), and linear dual-pol with (63-71%).The Hybrid-pol data with different modes

found to be good for crop classification apart from fullypolarimetric data [22].

Lardeux, C., Frison, P.L., Tison, C., Souyris, J.C, have addressed the potential of the SVM algorithm for classifying the polarimetric SAR data. The authors have used L-band, P-band, and C-band data in this study and have obtained an OA of 87%, 82%, and 99%, respectively. SVM classifier has recorded a great improvement of about 20% compared to Wishart classification [23].

Yekkehkhany, B., A. Safari, S. Homayouni, and M. Hasanlou have presented a comparative studyon the classification of multi-temporal L-band SAR data using different SVM kernels. In this study, the authors have opted for kernel functions such as RBF, Linear, and Polynomial. RBF Kernel performed better than the other two kernels. They have concluded that using two data OA increased by 14%, and byusing three multi-temporal data, OA increased by 5%. Moreover, the effect of multi-temporal data is expensive and time-consuming [24].

1.8 Research Objectives

The thesis deals with the three main applications of Microwave Remote sensing Viz. Land Use LandCover, Urban Land Cover, and Crop Discrimination.

(i) The first objective is to draw the Importance of Speckle filtering and the impact of speckle filterwindow size on speckle reduction in SAR images.
(ii) The second objective is to characterize the ground targets of Compact polarimetry data usingrobust m-chi and m-delta decomposition.
(iii) The third objective is to improve the overall classification accuracy of Hybrid-pol data usingvarious machine learning algorithms.
(iv) The fourth objective of this study is to explore the potential of compact polarimetry and compareit with other compact polarimetry modes.
(v) The fifth objective is to record, compare, and analyze the response of circular transmission overlinear transmission and its interaction with the targets.
(vi) The sixth objective is to compare the penetration capability and information content of L-bandAlos Palsar-2 and C-band RISAT-1 data.

1.9 Thesis Organization

The thesis is organized into seven chapters. The first chapter presents the introduction, background, motivation for the research work, problem statement, and literature survey. The second, third, and fourthchapters and fifth provide the contributions of the research work.

The sixth chapter provides theconclusions of the research work. The summary of each chapter is given below.

- Chapter 1: The First chapter deals with the introduction to Microwave Remote Sensing, and RadarPolarimetry. The motivation for the research is explained and the corresponding problem statement is derived. A literature survey is carried out for the problem statement identified.
- Chapter 2: The Second Chapter deals with the importance of speckle filtering and the effect of speckle window size on speckle reduction. Polarimetric Speckle filters preserve the information without a smoothing effect. Dual-pol, Hybrid-pol, Quad-pol, and Psuedo Quad pol data were usedfor speckle filtering for various land targets [25-38].
- Chapter 3: The Third Chapter deals with the Target Decomposition theorems which characterizesthe targets. In this chapter, a Four-component decomposition along with the robust m-delta and m-chi decomposition are explained in detail [39-56].
- Chapter 4: The Fourth Chapter deals with improving the classification accuracy on Hybrid-pol data using Supervised clasifier. In this chapter, an SVM parameterization effect on classificationaccuracy will be discussed in detail. A comparison of SVM classifier with Wishart classifier andother machine learning algorithms will be analyzed [57-70].
- Chapter 5: The Fifth Chapter deals with Exploring the Capability of Compact Polarimetry over other modes [71-92].
- Chapter 6: The sixth chapter deals with a comparison of Hybrid-Pol, C band RISAT-1 data over dual-pol and quad-pol for Land Cover Classification and Crop Identification [92-95].
- Chapter 7: A summary of the contributions and the conclusions drawn from the earlier chapters were discussed. The future extension of the proposed work is also discussed.

1.10 Imaging modes

SAR Images in three different modes depending on the application and the user requirement as shownin Fig 1.11 and Table 1.3.

Stripmap SAR: In this mode, the antenna pointing direction is constant as the radar platform moves. Thebeam sweeps along the ground at an approximately uniform rate, and a contiguous image is formed. A strip ground is imaged, and the length of the strip is only limited by how far the sensor moves or how long the radar is left on. The azimuth resolution is governed by the antenna length.

Scansar: This mode is a variation of stripmap SAR, whereby the antenna is scanned in range several times during a synthetic aperture. In this way, a much wide swath is obtained, but the azimuth resolutionis degraded (or the number of looks is reduced). The best azimuth resolution can be obtained in that of the stripmap mode multiplied by the number of swaths scanned.

Spotlight: The resolution of the stripmap mode can be improved by increasing the angular extent of the illumination on the area of interest (a spot on the ground). This can be done by steering the beam graduallybackwards as the sensor passes the scene. The beam steering has the transient effect of simulating a widerantenna beam (i.e., a shorter antenna). However, the antenna must ultimately be steered forward again,and a part of the ground is missed. This means that the coverage is not contiguous; only one spot on theground is imaged at a time.

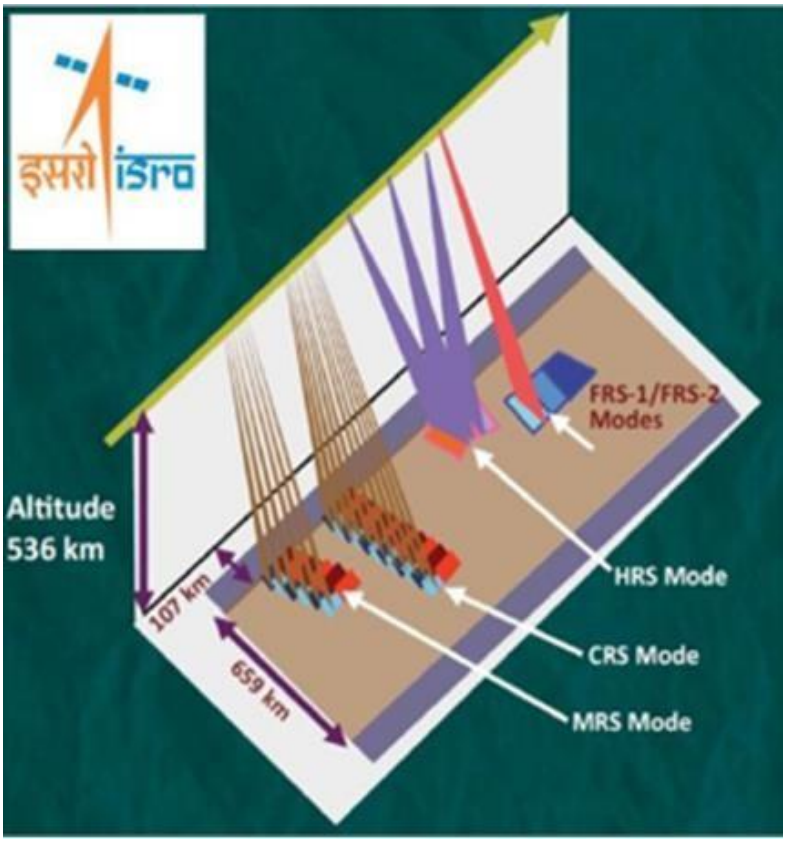

Fig 1.11 RISAT-1 Imaging Modes © ISRO

Mode	HRS	FRS-1	FRS-2	MRS	CRS
swath	10m	25km	25km	115km	223
Pol	Single, Dual, Circular	Single, Dual, Circular	Quad circular	Single, Dual, Circular	Single, Dual, Circular
Resolution	1*1(m)	3*2(m)	9*4 (m)	21-23*8 (m)	41-55*8 (m)
	spotlight mode	Stripmap	stripmap	Scansar	scansar

Table 1.3 Acquisition Modes of RISAT-1, The datasets and study area used in this work is shown

1.11 Datasets and Study Area

Dataset	Band	Date of Acquisition	Acquisitionmode	Resolution
RISAT-1 (Ghanpur Vil, Warangal Dst,Telangana, India. Compact polDual-pol	C C	5-07-2016 5-12-2015	FRS-1 FRS-1	3 meters

RISAT-1 (Hyderabad),IndiaHybrid Quad	C	29-09-2016 26-09-2014	FRS- 1 FRS- 1 FRS- 2	3 meters
Alos Palsar -1 (Hyderabad) Alos Palsar-2 (Sanfransico, MtFuji, Tokyo)	L	23-08-2010	Dual-pol Quad- pol	Better than 1meter
Sentinel 1A, 1B(Chennai), India	C	18-12-16	Dual-pol	

Table 1.4 Datasets and Study Area

1.12 Land Use and Land Cover (LULC)

Land cover: physical and biological cover of earth surface including artificial surfaces, agriculture areas,forests, wetlands, water bodies.

Land use: territory characterized according to its current and feature planned dimensions or socio-economic purpose (residential, commercial industrial, agriculture, forestry).

1.13 Scientific tool used for processing

- Envi SARscape [103]
- PolSARpro [104]

CHAPTER 2

PRE-REQUISITES

2.1 Raw SAR image product type and information

Sentinel-1 data products acquired in SM, IW and EW mode which are generated by the PDGS operationally are distributed at three levels of processing.

Level-0

Level-1

Level-2.

Level-1 products can be one of two product types - either Single Look Complex (SLC) or Ground Range Detected (GRD). Level-2 Ocean (OCN) products can have different components available depending on the acquisition mode.Products are designated based on their acquisition mode, product type and in the case of Level-1 GRD also its resolution.All products are processed directly from the Level-0 product. Each mode can potentially generate Level-1 SLC, Level-1 GRD and Level-2 Ocean products. For WV mode, the Level-0 products are not distributed; the access to WV_SLC product has been possible since 2016.

Level-0

The SAR Level-0 products consist of compressed and unfocused SAR raw data. Level-0 products are the basis from which all other high level products are produced. Level-0 data is compressed using Flexible Dynamic Block Adaptive Quantization (FDBAQ) which provides a variable bit rate coding that increases the number of bits allocated to bright scatterers. For the data to be usable, it will need to be decompressed and processed using focusing software Level-0 data includes noise, internal calibration and echo source packets as well as orbit and attitude information. Level-0 products are stored in the long term archives. They can be processed to generate any type of product during the mission lifetime and for 25 years after the end of the space segment operations. Level-0 products are available to data users for only the SM, IW and EW modes.

Level-1

Level-1 focused data are the products intended for most data users. The Level-0 product (raw data) is transformed into a Level-1 product by the Instrument Processing Facility (IPF) via the application of various algorithms as indicated below. These Level-1 products form a baseline product from which Level-2 products are derived.

The processing steps involved to produce Level-1 data products include pre-processing, Doppler centroid estimation, single look complex focusing, and image and post-processing for generation of the SLC and GRD products as well as mode specific processing for assembling of multiple sub-swath products.

Level-1 Processing Flow

For converting digital pixel values to radiometrically calibrated backscatter, all the required information can be found in the product. A calibration vector is included as an annotation in the product allowing simple conversion of image intensity values into sigma or gamma nought values. Further details of how to calibrate Sentinel-1 Level 1 products can be found in the 'Radiometric Calibration of S-1 Level-1 Products Generated by the S-1 IPF' document ESA-EOPG-CSCOP-TN. Level-1 data can be processed into either Single Look Complex (SLC) and/or Ground Range Detected (GRD) products. SLC products preserved phase information and are processed at the natural pixel spacing whereas GRD products contained the detected amplitude and are multi-looked to reduce the impact of speckle.

Single Look Complex

Level-1 Single Look Complex (SLC) products consist of focused SAR data, geo-referenced using orbit and attitude data from the satellite, and provided in slant-range geometry. Slant range is the natural radar range observation coordinate, defined as the line-of-sight from the radar to each reflecting object. The products are in zero-Doppler orientation where each row of pixels represents points along a line perpendicular to the sub-satellite track. The products include a single look in each dimension using the full available signal bandwidth and complex samples (real and imaginary) preserving the phase information. The products have been geo-referenced using the orbit and attitude data from the satellite and have been corrected for azimuth bi-static delay, elevation antenna pattern and range spreading loss. SM SLCs contain one image per polarisation for its single swath. IW, having three sub-swaths, has three images in single polarisation and six images for dual polarisation. EW, having five sub-swaths, has five images for single polarisation and ten images for dual polarisation products. For IW and EW, each sub-swath consists of a series of bursts in azimuth. The individually focused complex burst data are included, in azimuth-time order, into a single sub-swath image, with black-fill demarcation in between.

For IW, a focused burst has a duration of ~2.75 seconds and a burst overlap of approximately ~0.4 seconds. For EW, a focused burst has a duration of ~3.19 seconds with an overlap of ~0.1 seconds. The overlap slightly increases in range within a sub-swath. This overlap is sufficient to provide contiguous coverage of the ground. Images for all bursts in all sub-swaths of IW/EW SLC products are re-sampled to a common pixel spacing grid in range and azimuth. Burst synchronisation is maintained for both IW and EW products to ensure that interferometry between pairs of products acquired multiple repeat periods apart can be performed. The Swath Timing data set record in SLC products contains information about the bursts including dimensions, timing and location that can be used to merge the bursts and swaths together.

Ground Range Detected

Level-1 Ground Range Detected (GRD) products consist of focused SAR data that has been detected, multi-looked and projected to ground range using the Earth ellipsoid model WGS84. The ellipsoid projection of the GRD products is corrected using the terrain height specified in the product general annotation. The terrain height used varies in azimuth but is constant in range (but can be different for each IW/EW sub-swath). Ground range coordinates are the slant range coordinates projected onto the ellipsoid of the Earth. Pixel values represent detected amplitude. Phase information is lost. The resulting product has approximately square resolution pixels and square pixel spacing with reduced speckle at a cost of reduced spatial resolution. For the IW and EW GRD

products, multi-looking is performed on each burst individually. All bursts in all sub-swaths are then seamlessly merged to form a single, contiguous, ground range, detected image per polarisation.

Level-2

Level-2 consists of geolocated geophysical products derived from Level-1. Level-2 Ocean (OCN) products for wind, wave and currents applications may contain the following geophysical components derived from the SAR data:

Ocean Wind field (OWI)

Ocean Swell spectra (OSW)

Surface Radial Velocity (RVL)

The availability of components depends on the acquisition mode. The metadata referring to OWI are derived from an internally processed GRD product, the metadata referring to RVL (and OSW, for SM and WV mode) are derived from an internally processed SLC product. The OWI component is a ground range gridded estimate of the surface wind speed and direction at 10 m above the surface, derived from SM, IW or EW modes.

2.2 Pre-Processing Steps

The two Sentinel-1 satellites 1A and 1B are one of the first satellites which are providing microwave data in high temporal and spatial resolution. Within the MULTIPLY project we developed a preprocessing chain to process timeseries of Sentinel-1 data for quantitative analysis of vegetation and soil parameters over agricultural fields. Therefore, rigorous geometric and radiometric corrections as well as a multi-temporal speckle filter is applied. The different preprocessing steps are shown in Fig. 3.1 and Fig. 3.2. Furthermore, every processing step is explained in more detail in the following subsections. As it can be seen Fig. 3.1 and Fig. 3.2 the preprocessing work-flow is split in two main parts. The preprocessing methods in Fig. 3.1 can be applied separately for every image. Whereas the work-flow shown in Fig. 3.2 need several images which were preprocessed by the different steps presented in Fig. 3.1. The whole preprocessing chain for Sentinel-1 Level-1 Single Look Complex (SLC) data is accomplished by ESA's SNAP S1TBX software (current version 5.0.4). The SNAP toolbox can be downloaded from http://step.esa.int/main/ download/. However, to automatically apply different preprocessing steps on Sentinel-1 data a python script, which uses the Graph Processing Tool (GPT) of the S1TBX, is provided.

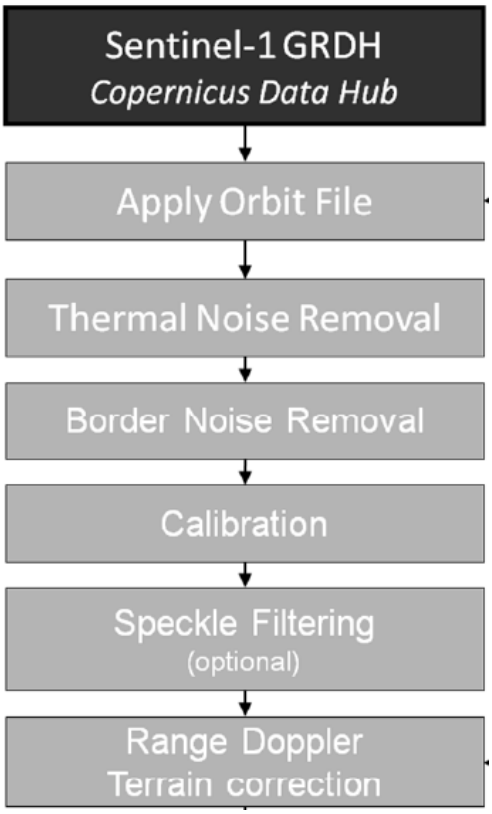

Subset:The raw image is much larger than what we need to process, so to make the processing require less resources, it is important that we first extract a subset from the image. This step could be skipped, but processing the entire scene is unnecessary and time consuming.

Orbit file: Before any SAR pre-processing steps occur, the product subset should be properly orthorectified to improve accuracy. To properly orthorectify the image, the orbit file is applied using the Apply-Orbit-File GPF module. SNAP is able to generate and apply a high accuracy satellite orbit file to a product. **:** The raw image is much larger than what we need to process, so to make the processing require less resources, it is important that we first extract a subset from the image. This step could be skipped, but processing the entire scene is unnecessary and time consuming. Orbit state vectors, contained within the metadata information of SAR products, are generally not accurate. The precise orbits of satellites are determined after several days and are available days-to-weeks after the generation of the product. The operation of applying a precise orbit available in SNAP allows the automatic download and update of the orbit state vectors for each SAR scene in its product metadata, providing an accurate satellite position and velocity information.

Thermal Noise Removal: Sentinel-1 image intensity is disturbed by additive thermal noise, particularly in the cross-polarization channel. Thermal noise removal reduces noise effects in the inter-sub-swath texture, in particular, normalizing the backscatter signal within the entire Sentinel-1 scene and resulting in reduced discontinuities between sub-swaths for scenes in multi-swath acquisition modes. The thermal noise removal operator available in SNAP for Sentinel-1 data can also re-introduce the noise signal that could have been removed during level-1 product generation, and update product annotations to allow for re-application of the correction [3]. Sentinel-1 level-1

products provide a noise look-up table (LUT), provided in linear power, for each measurement data set and used to derive calibrated noise profiles matching the calibrated GRD data

Border Noise Removal : While generating level-1 products, it is necessary to correct the sampling start time in order to compensate for the change of the Earth's curvature. At the same time, azimuth and range compression leads to radiometric artefacts at the image borders. The border noise removal algorithm [4], available as an operator in SNAP, was designed in order to remove low intensity noise and invalid data on scene edges.

CALIBRATION : With our data now properly ortho rectified with a high-quality generated orbit file, it is now time to calibrate the data to sigma-naught values. The data is now stored in a band called Sigma0_VV in the product object product calibrated with a much smaller range of values.

Radiometric Calibration: Radiometric calibration is applied to correct for the bias of SAR data products. The required absolute calibration factor is derived by measuring the SAR system against reference point targets with well-known radar cross section (transponders and corner reflectors) together with reference distributed targets such as the Amazon rainforest. As the requirement on the radiometric accuracy is 1 dB (3σ) in all four operational modes, it is necessary for multiple measurements to be made for each SM swath and for each IW/EW sub-swath and for each polarisation.

Polarimetric Calibration: External calibration devices can also be used to measure polarimetric co-registration and polarimetric channel distortion (cross-talk). The co-registration assessment is based on the IRF peak pixel position of the transponders in both polarisations of dual polarisation products. Unlike transponders, a standard type of corner reflector (trihedral) will only have a response in HH or VV and so an IRF response will be seen in only one of the polarisations in the dual-polarisation L1 products. Although unsuitable for co-registration analysis, an assessment of cross-talk can be made using this type of calibration device.

Elevation Antenna Pattern Verification: Antenna model verification ensures the provision of precise reference elevation antenna patterns of all operation modes and the gain offset between different beams. Verification of the antenna model is performed by comparison with Elevation Antenna Patterns (EAPs) derived from imagery of the large isotropic distributed target of the Amazon rainforest. Verification is performed for all possible polarisation combinations.

Polarimetric Calibration: External calibration devices can also be used to measure polarimetric co-registration and polarimetric channel distortion (cross-talk). The co-registration assessment is based on the IRF peak pixel position of the transponders in both polarisations of dual polarisation products. Unlike transponders, a standard type of corner reflector (trihedral) will only have a response in HH or VV and so an IRF response will be seen in only one of the polarisations in the dual-polarisation L1 products. Although unsuitable for co-registration analysis, an assessment of cross-talk can be made using this type of calibration device.

Geometric Calibration: Geometric calibration is required to accurately locate a pixel position in an image to the geographic location on the Earth's surface. This is achieved using the surveyed

location of reference targets such as corner reflectors. Comparison with the surveyed and measured location of the reference targets are used to measure both range and azimuth timing biases that can subsequently be included in the SAR processor. To enable this comparison to be performed various corrections, such as the atmospheric path delay, are required using various external information (meteorological, plate tectonic and solid Earth tide).

Antenna Pointing Determination: Antenna pointing determination is performed to achieve correct beam pointing of the antenna in both azimuth and elevation. The azimuth pointing is determined using the receiver mode of transponders while in elevation a special notch acquisition is performed over the Amazon rainforest.

SPECKLE FILTERING

Speckle is a granular interference that inherently exists in and degrades the quality of the, synthetic aperture radar (SAR) images.The speckle effect is a result of the interference of many waves of the same frequency, having different phases and amplitudes, which add together to give a resultant wave whose amplitude, and therefore intensity, varies randomly. If each wave is modeled by a vector, then it can be seen that if a number of vectors with random angles are added together, the length of the resulting vector can be anything from zero to the sum of the individual vector lengths—a 2-dimensional random walk, sometimes known as a drunkard's walk. In the limit of many interfering waves, and for polarised waves, the distribution of intensities (which go as the square of the vector's length) becomes exponential.A speckle pattern is produced by the mutual interference of a set of coherent wavefronts.

$$P(I) = \frac{1}{\langle I \rangle} \exp\left(\frac{-I}{\langle I \rangle}\right)$$

The speckle noise appearing in SAR images forms a main obstacle to analyse, interpret and classify SAR images for various remote sensing applications. To date, many filters have been developed for speckle reduction in SAR imagery. In this paper, the authers evaluate eight ready-made speckle filters, which are Moving Average Filter, Median Filter, Lee Filter, Enhanced Lee Filter, Frost Filter, Enhanced Frost Filter, Kuan Filter and Gamma MAP filter

The speckle filtering techniques can be classified into two categories[6]. The techniques in the first category are equivalent to applying a low-pass filter to the image, such as multi-look processing and the box filter. This step is taken as a part of preprocessing. The second category is to reduce speckle noise after the SAR image has been formed. It is considered as a part of the post-processing of SAR images.

Here only the filters for the second category are discussed as follows,

1. Box Filter : It is a typical low-pass filter, which can remove the noise with a high frequency spectrum as well as smoothing the details, such as the edges and points etc.

2. Median Filter: It is a nonlinear filter and is derived from the maximum-likelihood (ML) estimation principle by assuming the signal to be contaminated by additive noise with a Laplace distribution. In some cases, it is much more efficient than most other filters.

3. Lee Filter: It was derived from the minimum square error(MMSE) criteria by introducing the local statistics method in it. It was believed that it can reduce speckle noise while preserving the edges in the image.

4. Frost Filter: It was also derived from the principle of MMSE. The filter kernel can vary with the local statistical value of the images so as to reduce the noise while at the same keeping the edges.

5. Kuan Filter: It is derived from MMSE criteria under the assumption of a nonstationary mean and nonstationary variance(NMNV). It is quite similar to the Lee Filter in form. However, it is considered to be aa little more accurate than Lee Filter due to the fact that no approximation is required in the total derivation.

6. Enhanced Lee Filter:Based on the Lee filter, A.Lopes modified it to improve the ability of preserving the edges in the image.

7. Enhanced Frost Filter:The similar modification as Enhanced Lee Filter was introduced to the Frost Filter.

8. Gamma MAP Filter:It is derived under the assumption of the image scene having a Gamma Distribution, which is believed more suitable to the realistic case.

Filter	Weighting Function	Filtering Formula
Box	$W(x,y)=\begin{cases}1 & \lvert x\rvert\le x_0 \quad \lvert y\rvert\le y_0\\ 0 & otherwise\end{cases}$	$\hat{I}=I*W$
Median		$\hat{I}=\underset{\lvert x\rvert\le x_0,\lvert y\rvert y_0}{Median}(I(x,y))$
Lee	$W(x,y)=1-\frac{C_{si}^2}{C_I^2(x,y)}$	$\hat{I}=I\cdot W+\bar{I}(1-W)$
Frost	$W(x,y)=K_1e^{-K_dC_I(x,y)\sqrt{x^2+y^2}}$	$\hat{I}=I*W$
Kuan	$W(x,y)=\frac{1-C_{si}^2/C_I^2(x,y)}{1+C_{si}^2}$	$\hat{I}=I\cdot W+\bar{I}(1-W)$
Enh. Lee	$W(x,y)=e^{-K_d\frac{C_I(x,y)-C_{si}}{C_{max}-C_I(x,y)}}$	$\hat{I}=\bar{I} \quad C_I\le C_{si}$ $\hat{I}=I\cdot W+\bar{I}(1-W)$ $C_{si}<C<C_{max}$ $\hat{I}=I \quad C_I\ge C_{max}$
Enh. Frost	$W(x,y)=K_1e^{-K_d\frac{C_I(x,y)-C_{si}}{C_{max}-C_I(x,y}\sqrt{x^2+y^2}}$	$\hat{I}=\bar{I} \quad C_I\le C_{si}$ $\hat{I}=I*W \quad C_{si}<C<C_{max}$ $\hat{I}=I \quad C_I\ge C_{max}$
GMAP	where $k=\alpha-N-1$ $\alpha=\frac{1+C_{si}}{C_I^2-C_{si}^2}$	$\hat{I}=\bar{I} \quad C_I\le C_{si}$ $\hat{I}=\frac{k\bar{I}+\sqrt{\bar{I}^2k^2+4\alpha N\bar{I}}}{2\alpha}$ $C_{si}<C<C_{max}$ $\hat{I}=I \quad C_I\ge C_{max}$

Table 2.1 Formula for several filters

Where Ci is standard speckle index, C, is varied standard speckle index, N is the number of looks, Cmax is the upper threshold and K, is called damping factor.

CHAPTER 3

Literature survey

3.1 Detection of Flood Prone Areas by Flood Mapping of SAR Imagery

Floods have catastrophic consequences including loss of human life and devastating damage to property. In India, floods are a frequent occurrence in monsoon in several parts of the country. Statistics show that almost 12% of India's land area is prominently prone to floods. In the past 65 years, India has suffered losses worth more than INR 3.7 Lakh Cr. due to flooding. Rivers in India crossed their highest flood level no less than 25 times in August 2019 alone. The flash floods of Mumbai on 26th July 2005 and the Uttarakhand floods of 2013 serve as stark reminders about the severity of floods. Therefore, the need to have a system which can accurately chalk out flood-prone areas beforehand is of prime importance in today's scenario.

Flood mapping is a vital cog in the wheel of flood risk management. It is a ground truth mapping based process for identifying areas at risk of flooding on a map. It is useful to minimize the damage to life and property and for estimating flood risk.
Synthetic aperture radar is a radar type which has a unique and distinctive feature of using relative motion to an antenna to give distinguishable long-range coherent signals that are further dissipated to produce a very fine spatial resolution.

It is not possible to attain such finesse with standard beam scanning means.
Our study aims to create a procedure which can identify regions that are prone to flooding and serve as an early warning/precaution system for the locals as well as the government officials. Locals can be better warned of being wary of flooding and take necessary precautions to prepare for the situation or vacate the area thus preventing disastrous situations and reduce the resulting damage. Officials once warned of any area's high probability of flooding can then assess and accordingly take measures to prevent a disastrous situation

3.2 Flooding Extent Mapping for Synthetic Aperture Radar Time Series Using River Gauge Observations

The flooding extent area in a river valley is related to river gauge observations such as discharge and water elevations. The higher the water elevations, or discharge, the larger
the flooding area. Flooding extent maps are often derived from synthetic aperture radar (SAR) images using thresholding methods. The thresholding methods vary in complexity and number of required parameters. We proposed a simple thresholding method that takes advantage of the correlation between the river gauge and the flooding area. To show the applicability of the method, we used a 2014–2018 time series of 161 Sentinel 1 SAR images acquired over a wetland floodplain located in Northeast Poland. We validated themethod by extracting local water line elevations from a high-resolution digital elevation model for three river gauges, which resulted in a root-mean-square error of 0.16 m, a bias of 0.07 m, and a correlation of 0.86 for the best scenario. The scenario analysis showed that the most important factor affecting the method's accuracy was a proper delineation of the zone inwhich the flooding extent area was calculated. This was because other water sources,

uncorrelatedwith river flow, were present in the floodplain as open water. Additionally, higher accuracy was obtained for the VV than VH polarization. The discharge can be used instead of water elevations as a river gauge variable, but this results in more
bias in the water extent estimates.

Flooding extent maps developed using satellite synthetic aperture radar (SAR) data have been providing valuable information for crisis response, ecology, or hydraulic modeling. So far, many methods have been developed, of which the most popular choose the radar backscatter threshold below which a SAR data pixel is labeled as flooded either in an automated way [1], or by expert judgment . These simple robust methods have limited applicability in difficult case studies, such as with complex topography or abundant vegetation, and therefore were modified or adapted in more complex methods. Recentexamples of complex flood mapping methods used ancillary data and region growing , local correction algorithms of radar layover, and emergent vegetation , elevation-based filtering and processing in local tiles , or classification, including multistep classification, often followed by data transformation. The disadvantages of complex methods are limited repeatability due to a lack of ready-to-use software and the need to provide parameter values (for some of the methods). Long-term SAR sensor missions, such as PALSAR, Radarsat, and Sentinel 1, provide an opportunity to produce flooding map time series, which have been utilized in studies focusing on flood monitoring and ecology . The time series has also been very useful for hydrodynamic model calibration and validation A deeper analysis of the time-series approach revealed that high spatial resolution of SAR data is more important than its temporal resolution in model calibration. Moreover, the uncertainty of roughness parameters (one of the most important parameters of hydrodynamic models) is lower when the model is calibrated with SAR images taken before rather than during or after the flood peak . These findings highlight the benefits of using high-spatial- and temporal-resolution flooding extent maps, which nowadays can be elaborated using contemporary SAR sensors. Yet, as discussed before, more complex methods, which were often used for the elaboration of SAR flooding extent time series, are more difficult to use than simple robust methods. In contrast, simple methods lack features for automatic processing SAR data time series, which may lead to inconsistencies between the flood extents derived from subsequent images. To overcome this issue, a method that relates time series of SAR data with another observed variable, related to flooding extent, can be used. Flooding extent maps were used to derive time series of river discharge estimates in several British Columbia (Canada) and South Korea rivers. Another approach was to relate water depth in the Congo River (Africa) with SAR backscatter using satellite altimeter data instead of river gauge for observation . Flooding extent maps were also used to derive a relation between water elevation and river extent for dike location prediction in two United Kingdom rivers . These kinds of relations can be used conversely—to derive flooding extents using observed water elevations or discharges. In a preliminary study, this approach was used to estimate the backscatter threshold for flood mapping using a series of 120 SAR images and discharge observation in the Biebrza River wetland floodplain (Poland) [26]. That study used a search technique to find the optimal threshold by maximizing the correlation between flooding area and discharge. Effectively, the optimal correlation coefficient was 0.59, and a reasonable flooding extent was provided when compared to color-infrared satellite images. However, that study also indicated the limitation of this technique during wet conditions in the floodplain (i.e., when water from other sources than the river is present) and the requirement of deeper validation. In this study, we aim to perform further tests of an automated method for the radar backscatter threshold estimation using SAR imagery and observed hydraulic variables. We seek to investigate the effects of the polarization used (VV or VH), the extent of the zone used for calculation of the flooding extent area, and the observed hydraulic variable used, i.e., dischargeor water elevations.We also perform validation of the estimated flooding extents by extracting the water line elevation in the neighborhood of three

gauging stations. Finally, we discuss the method in the scope of providing data for integrated hydrological model validation.

3.3 Flood Mapping With SAR And Multi-Spectral Remote Sensing Images Based On Weighted Evidential Fusion

Synthetic Aperture Radar (SAR) and Multi-spectral (MS) remote sensing images are commonly used for flood mapping. SAR images can provide valid backscattering measurements of inundated areas through cloud cover, while MS data is able to monitor the spectral changes of ground surface, but usually affected by clouds. The complementary characteristics of the two data indicate the potential of their combining application for flood monitoring in emergency. This paper proposes a novel weighted evidential fusion method to take full advantages of the SAR and MS data for change detection during the flood. First, pre-processing and classification are performed with the SAR and MS data, independently. Second, a modified PCR6 rule for evidential fusion is proposed, which introduces the confusion matrixes to calculate the weight of evidences so that the conflicting degree in the fusion process can be reduced. Then, the flood inundating, standing and receding patterns are identified, which can be used to describe the flooding process in details. Practically, the proposed method is applied to flood mapping of the *Typhoon Rumbia* in 2018, in Shouguang City, China. The experiments show that the proposed fusion scheme efficiently use both of the SAR and MS data, and improve the flood mapping accuracy.

Rapid and accurate mapping of floods is important for flood prevention, emergency management, and post-disaster reconstruction [1]. The incremental big earth observation (EO) data and remote sensing techniques have demonstrated great potential in near-real time and synergistic flood mapping. Synthetic Aperture Radar (SAR) is particularly useful for
flood mapping especially in rainy or cloudy weather, because of its capability to monitor land surface changes in almost any weather conditions [2]. However, land surface water is not
always easy to be detected in SAR images when the water is stirred by storms (which lead to high surface roughness), covered by tall plants, or in topography shadows [3]. Multispectral
(MS) remote sensing images are complementary with the SAR data. MS images can be used to detect spectral changes of land surface resulting from water coverage. However, clouds or shadows are usually considered as defective information, and limits their application on flood
mapping using multi-temporal MS data [4]. Hence, the combining use of SAR and MS satellite imagery can be prospective and effective for inundation detection and flood mapping. Many methods have been proposed for mapping flood inundation only use SAR or MS images [2]. However, the combining use of SAR and MS images for flood mapping, especially for detecting the flood inundating, standing, and receding patterns with multi-temporal data is still challenging. The main difficulty lies on the uncertainty and conflicting
information that exist between the SAR and MS data. The evidential fusion method, generally known as a fusion scheme on the decision level, can flexibly combine multiple imprecise or uncertain evidences and has been successfully applied to change detection with multi-source remote sensing data in emergency situations [5]. Even though the method is usually more effective than the traditional Bayesian ones, the existing evidential fusion algorithms neglect the difference of overall accuracy of the evidences, and lead to low accuracy when fusing multi-source data with high conflict degree [6]. This research develops an innovative weighting scheme based on PCR6 rule of the evidential fusion method using multi-temporal SAR and MS images, and applies the method to detect the inundating, standing, and receding patterns in the whole flooding process.

3.4 Sentinel-1-Based Water and Flood Mapping: Benchmarking Convolutional Neural Networks Against an Operational Rule-Based Processing Chain

In this study, the effectiveness of several convolutional neural network architectures (AlbuNet-34/FCN/DeepLabV3+/UNet/ U-Net++) for water and flood mapping using Sentinel-1 amplitude data is compared to an operational rule-based processor (S-1FS). This comparison is made using a globally distributed dataset of Sentinel-1 scenes and the corresponding ground truth water masks derived fromSentinel-2 data to evaluate the performance of the classifiers on a global scale in various environmental conditions. The impact of using single versus dual-polarized input data on the segmentation capabilities ofAlbuNet-34 is evaluated. The weighted cross entropy loss is combinedwith the Lovász loss and various data augmentation methods are investigated. Furthermore, the concept of atrous spatial pyramid pooling used in DeepLabV3+ and the multiscale feature fusion inherent in U-Net++ are assessed. Finally, the generalization capacity of AlbuNet-34 is tested in a realistic flood mapping scenario by using additional data fromtwo flood events and the Sen1Floods11 dataset. The model trained using dual polarized data outperforms the S-1FS significantly and increases the intersection over union (IoU) score by 5%. Using a weighted combination of the cross entropy and the Lovász loss increases the IoU score by another 2%. Geometric data augmentation degrades the performancewhile radiometric data augmentation leads to better testing results. FCN/DeepLabV3+/U-Net/U-Net++ perform not significantly different to AlbuNet-34. Models trained on data showing no distinct inundation perform very well in mapping the water extent during two flood events, reaching IoU scores of 0.96 and 0.94, respectively, and perform comparatively well on the Sen1Floods11 dataset.

The demand for reliable and robust crisis information after catastrophic disasters has substantially grown in the past decades [1]. Earth observation satellites are increasingly used to obtain reliable large-scale crisis information, owed to their ability of being almost independent of the underlying terrain, the possibility of acquiring data over large areas in a short amount of time and their different sensor systems. To provide the required information in a timelymanner, international initiatives such as the International Charter “Space and Major Disasters” have been founded, linking space agencies from all over the world and allowing a rapid disaster response by sharing the available satellite resources. Flood events make up one-third of all recorded natural disasters in the past century [2] and were related to approximately 52% of all activations of the International Charter “Space and Major Disasters” between the years 1999 and 2013 [1]. They are usually not localized but affect large regions simultaneously and the atmospheric conditions often prevent observation using optical or multispectral sensor systems. These preconditions make synthetic aperture radar

(SAR) an ideal sensor system to be used in flood emergency situations. SAR is a side-looking imaging radar system that utilizes microwave radiation to create images of the surface of the Earth. It is an active instrument that requires no illumination from the sun and can penetrate cloud cover, thus it is often used for rapid mapping purposes during flood events [1]. To derive the flood water extent from SAR data with a high accuracy, sophisticated data analysis steps are required. Visual scene interpretation and flood extent mapping are possible, but have several disadvantages. The areas usually affected by flood events are very large, which renders visual interpretation a very time-consuming task. Furthermore, the results depend on the skills and the subjective perception of an image interpretation expert, which poses a problem for reproducibility [3]. Hence, several semi-automatic and automatic approaches for flood extent mapping have been developed, often relying on thresholding as their core concept. Thresholding is a common technique used to classify every pixel of a SARimage into the classeswater or non-water. A pixel intensity threshold value that separates the two classes is chosen. Every pixel with an intensity value below that threshold is classified as water, all other pixels are classified as nonwater. The quality of the classification is strongly dependent on the contrast between water and nonwater pixels, which poses a problem for certain land cover types or water conditions (i.e., rough water surfaces, urban areas, sand patches)

CHAPTER 4

METHODOLOGY

4.1 Software Implementation

4.1.1 Importing needed modules in python

1.Snap.py:

Snap.py is a Python interface for SNAP. SNAP is a general purpose, high performance system for analysis and manipulation of large networks. SNAP is written in C++ and optimized for maximum performance and compact graph representation. It easily scales to massive networks with hundreds of millions of nodes, and billions of edges.Snap.py provides performance benefits of SNAP, combined with flexibility of Python. Most of the SNAP functionality is available via Snap.py in Python.The latest version of Snap.py is 6.0 (Dec 28, 2020), available for macOS, Linux, and Windows 64-bit. This version is a major release with a large number of new features, most notably a significantly improved way to call Snap.py functions in Python, a NetworkX compatibility layer, standard Python functions to handle SNAP vector and hash types, new functions for egonets and graph union, and a completely revised package building infrastructure with a better support for various versions of Python (see Release Notes for details). These enhancements are backward compatible, so existing Snap.py based programs should continue to work.

Snap.py can be installed via the pip module. To install Snap.py, execute pip from the command line as follows: python -m pip install snap-stanford

If you have more than one version of Python installed on the system, make sure that python refers to the executable that you want to install Snap.py for. You might also need to add --user after install, if pip complains about your adminsitrative rights. The most recent notes about installing Snap.py on various systems is available at this document: Snap.py Installation Matrix.

2.Numpy

NumPy is a Python library used for working with arrays.It also has functions for working in domain of linear algebra, fourier transform, and matrices. NumPy was created in 2005 by Travis Oliphant. It is an open source project and you can use it freely. NumPy stands for Numerical Python. In Python we have lists that serve the purpose of arrays, but they are slow to process.NumPy aims to provide an array object that is up to 50x faster than traditional Python lists.The array object in NumPy is called ndarray, it provides a lot of supporting functions that make working with ndarray very easy. Arrays are very frequently used in data science, where speed and resources are very important. NumPy arrays are stored at one continuous place in memory unlike lists, so processes

can access and manipulate them very efficiently. This behavior is called locality of reference in computer science. This is the main reason why NumPy is faster than lists. Also it is optimized to work with latest CPU architectures. NumPy is a Python library and is written partially in Python, but most of the parts that require fast computation are written in C or C++. you can install NumPy with:

pip install numpy

3.Matplotlib

Matplotlib is an amazing visualization library in Python for 2D plots of arrays. Matplotlib is a multi-platform data visualization library built on NumPy arrays and designed to work with the broader SciPy stack. It was introduced by John Hunter in the year 2002.One of the greatest benefits of visualization is that it allows us visual access to huge amounts of data in easily digestible visuals. Matplotlib consists of several plots like line, bar, scatter, histogram etc. Matplotlib was originally written by John D. Hunter. Since then it has an active development community and is distributed under a BSD-style license. Michael Droettboom was nominated as matplotlib's lead developer shortly before John Hunter's death in August 2012 and was further joined by Thomas Caswell. Matplotlib is a NumFOCUS fiscally sponsored project. Matplotlib 2.0.x supports Python versions 2.7 through 3.10. Python 3 support started with Matplotlib 1.2. Matplotlib 1.4 is the last version to support Python 2.6. Matplotlib has pledged not to support Python 2 past 2020 by signing the Python 3 Statement. Windows, Linux and macOS distributions have matplotlib and most of its dependencies as wheel packages. Run the following command to install matplotlib package : python -mpip install -U matplotlib

4.1.2 Reading the product

Reading in products with Snappy is simple - you do not even need to have the data unzipped. You'll need to download one dataset the Sentinel 1 product. The Sentinel 1 product can be accessed through Copernicus Scihub, the full product Name is S1A_IW_GRDH_1SDV_20211128T003147_20211128T003212_040764_04D697 _BA95. This is the product of the tirupati side region which is covered inside the polygon. We use product.ProductIO method from snappy to read the product. Its okay to give the whole zip file as is. ProductIO is capable to open zip files and read the data. We read the data with following command

product = ProductIO.readProduct(path_to_sentinel_data)

Fig 4.1 Raw data

4.1.3 Pre-Processing steps

1. Orbit file application

Before any SAR pre-processing steps occur, the product subset should be properly orthorectified to improve accuracy. To properly orthorectify the image, the orbit file is applied using the Apply-Orbit-File GPF module. SNAP is able to generate and apply a high accuracy satellite orbit file to a product. The orbit file provides accurate satellite position and velocity information. Based on this information, the orbit state vectors in the abstract metadata of the product are updated. The precise orbit files are available days-to-weeks after the generation of the product. Since this is an optional processing step, the tool will continue the workflow in case the orbit file is not yet available to allow rapid mapping applications.

2. Clipping/subsetting images

The raw image is much larger than what we need to process, so to make the processing require less resources, it is important that we first extract a subset from the image. This step could be skipped, but processing the entire scene is unnecessary and time consuming. To clip our image, the easiest way to do so is to convert a shape boundary file into a WKT (Well Known Text) string. If we look at the width and height of the subset, we can see that it is now a much smaller product than our original, with all the original bands still available. We can also display the subset using the plotBand method we defined earlier. With our image now subsetted to the area we want to run our analysis on, we now need to apply some preprocessing and corrections to the data. Our end goal is to determine flooding with delineation techniques - literature shows that the VV polarization has

advantages for flood delineation calculations over other polarizations, so we will apply processing on the VV intensity band.
The subsetted image is as shown below:

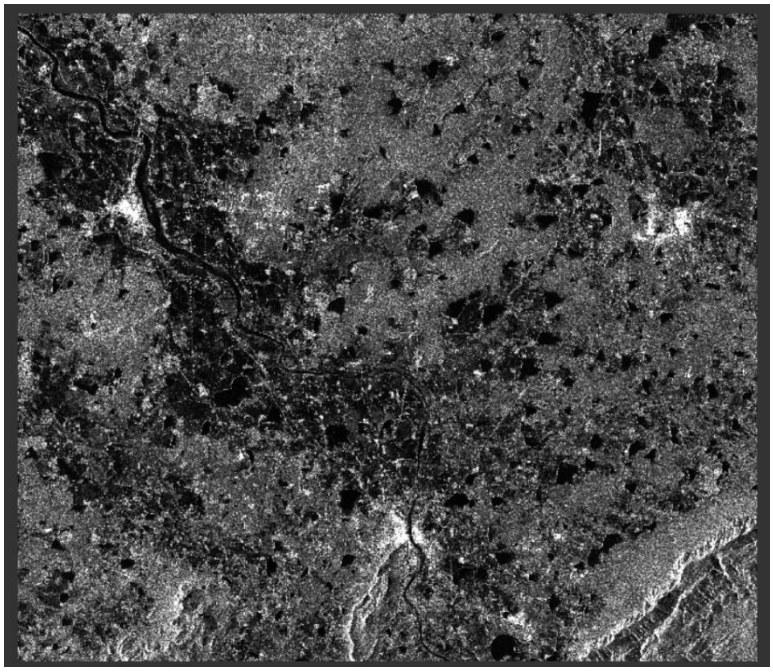

Fig 4.2 Subset

3. Image calibration

With our data now properly orthorectified with a high-quality generated orbit file, it is now time to calibrate the data to sigma-naught values. The data is now stored in a band called Sigma0_VV in the product object product_calibrated with a much smaller range of values.

4. Speckle filter

In the next pre-processing section, we must apply a speckle filter to our area of interest. This removes Speckle noise from the imagery. SAR images have inherent texturing called speckles which degrade the quality of the image and make interpretation of features more difficult. Speckles are caused by random constructive and destructive interference of the de-phased but coherent return waves scattered by the elementary scatter within each resolution cell. Speckle noise reduction can be applied either by spatial filtering or multilook processing. A Lee filter with an X, Y size of 5, 5 is used in this step.

5. Applying terrain correction

Finally, we must apply terrain correction to our product. Due to topographical variations of a scene and the tilt of the satellite sensor, distances can be distorted in the SAR images. Data which is not directly directed towards the sensor's Nadir location will have some distortion. Therefore, terrain corrections are intended to compensate for these distortions to allow a realistic geometric representation in the image.

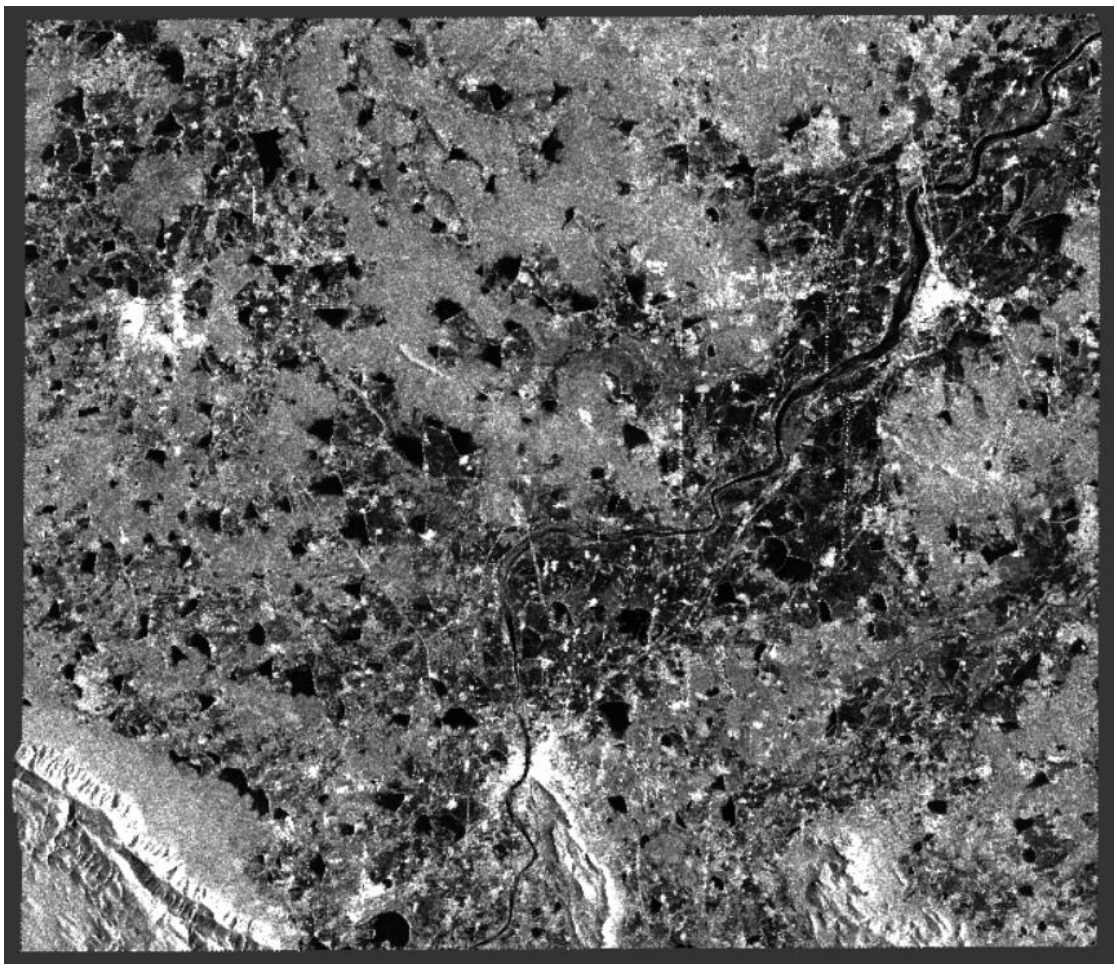

Fig 4.3 Pre-processed image

4.1.4 Binary flood masking and masking known water

1. Generating a binary flood mask

Since the current product we have processed contains backscatter coefficient values, pixels with a low backscatter will be flooded, while pixels with a high backscatter value will not be flooded. In order to obtain a binary flood mask, the histogram is analyzed to separate water from non-water pixels. Due to the side-looking geometry of SAR sensors and the comparably smooth surface of water, only a very small proportion of backscatter is reflected back to the sensor leading to comparably low pixel values in the histogram. The threshold used for separation is automatically calculated using scikit-image implementations and a combined use of the minimum method and Otsu's method. The GlobCover layer of the European Space Agency is used to mask out permanent water bodies. For this particular area, a threshold of 0.013 was found to be sufficient to separate areas affected by the flooding from the rest of the image. We can apply this threshold to generate a binary flood mask using the BandMaths GPF module.

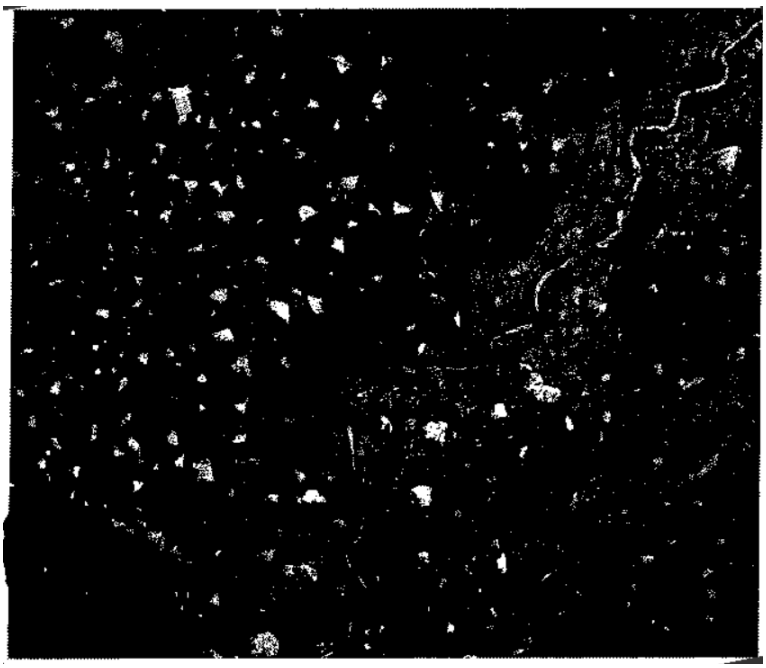

Fig 4.4 Binary flood mask showing all water bodies

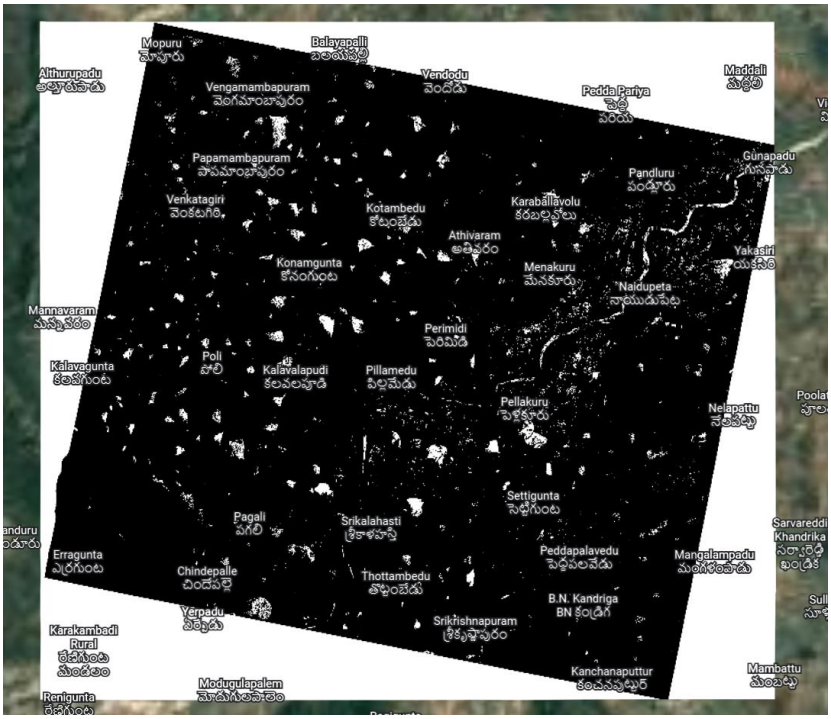

Fig 4.5 Same binary mask with reference to google earth

2. Masking out known water areas

Currently, our backscatter coefficient classification has misidentified inland bodies of water as flooded areas. These can easily be masked out by importing a land cover layer, converting it to a binary mask, and removing any values that are already known as water, such as the lake in the lower left hand corner of the island. To begin, we'll first use the AddLandCover GPF module to automatically download the GlobCover land use dataset for our study area.(http://due.esrin.esa.int/page_globcover.php). Our GlobCover layer is added as a band with the name land_cover_GlobCover.The classification scheme for GlobCover is as follows:

Label	..	Value
11 Post-flooding or irrigated croplands (or aquatic)		11
14 Rainfed croplands		14
20 Mosaic cropland (50-70%) / vegetation (grassland/shrubland/forest) (20-50%)		20
30 Mosaic vegetation (grassland/shrubland/forest) (50-70%) / cropland (20-50%)		30
40 Closed to open (>15%) broadleaved evergreen or semi-deciduous forest (>5m)		40
50 Closed (>40%) broadleaved deciduous forest (>5m)		50
60 Open (15-40%) broadleaved deciduous forest/woodland (>5m)		60
70 Closed (>40%) needleleaved evergreen forest (>5m)		70
90 Open (15-40%) needleleaved deciduous or evergreen forest (>5m)		90
100 Closed to open (>15%) mixed broadleaved and needleleaved forest (>5m)		100
110 Mosaic forest or shrubland (50-70%) / grassland (20-50%)		110
120 Mosaic grassland (50-70%) / forest or shrubland (20-50%)		120
130 Closed to open (>15%) (broadleaved or needleleaved, evergreen or deciduous) shrubland (<5m)		130
140 Closed to open (>15%) herbaceous vegetation (grassland, savannas or lichens/mosses)		140
150 Sparse (<15%) vegetation		150
160 Closed to open (>15%) broadleaved forest regularly flooded (semi-permanently or temporarily) - Fresh or brackish water		160
170 Closed (>40%) broadleaved forest or shrubland permanently flooded - Saline or brackish water		170
180 Closed to open (>15%) grassland or woody vegetation on regularly flooded or waterlogged soil - Fresh, brackish or saline water		180
190 Artificial surfaces and associated areas (Urban areas >50%)		190
200 Bare areas		200
210 Water bodies		210
220 Permanent snow and ice		220
230 No data		230

The value we want to include in our known water mask is 210. We can create our binary water mask by using code similar to what we used earlier to generate the flood mask. With our binary water mask created, it is time to mask out the lake and other small known water areas using it.

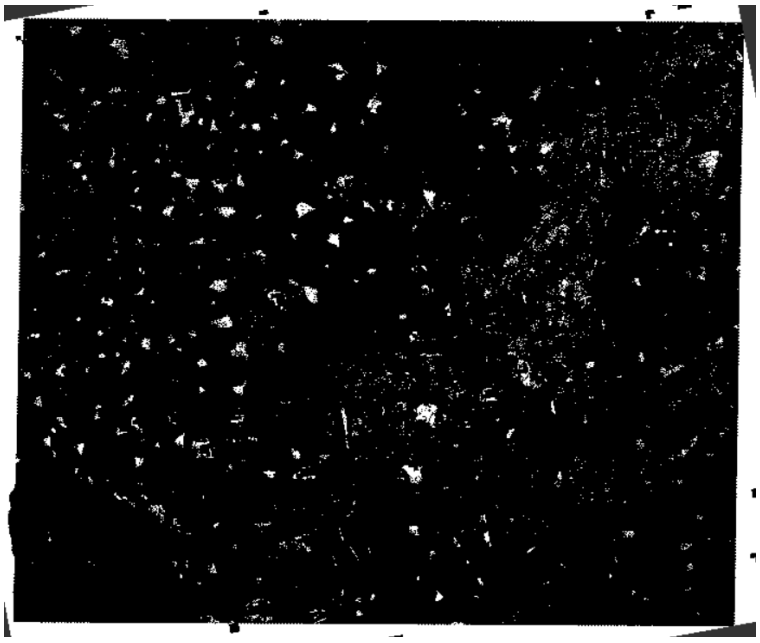

Fig 4.6 all the flooded region without normal water bodies

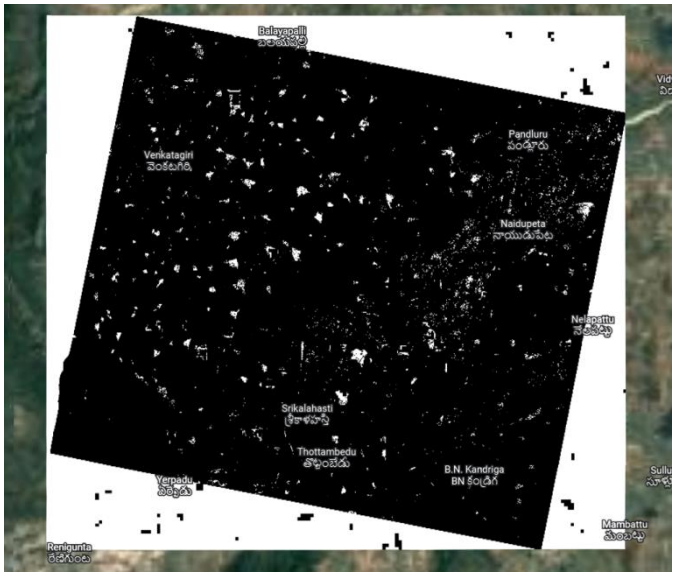

Fig 4.7 Same image with refeence to google earth

3. Saving the product

You can save the mask product (saves to data/final_mask.tif and then open it in SNAP or any other GIS/remote sensing platform with the following command:
ProductIO.writeProduct(water_mask2, "data/final_mask", 'kml')
We can save the file in many formats like beam dif, geotif, kml etc. In our case I saved it in kml file

CHAPTER 5

RESULT AND DISCUSSION

After masking known water we write the product as geotiff or beam dif file,which will look like the pictures below. All the white patches denote the water bodies, as we have masked the land based on the threshold .As we can see from the below pictures, the first picture is binary flood mask, which marks all the water bodies present in that area. We took the polygon around srikalahasti tirupathi region , which was flood prone in November 2021.You can see the overflowing swarnamukhi river and other ponds too in binary flood as it only marks water and masks out the land. But in the flooded picture you can clearly see the extra water bodies, which is flood water that is other than known water bodies.

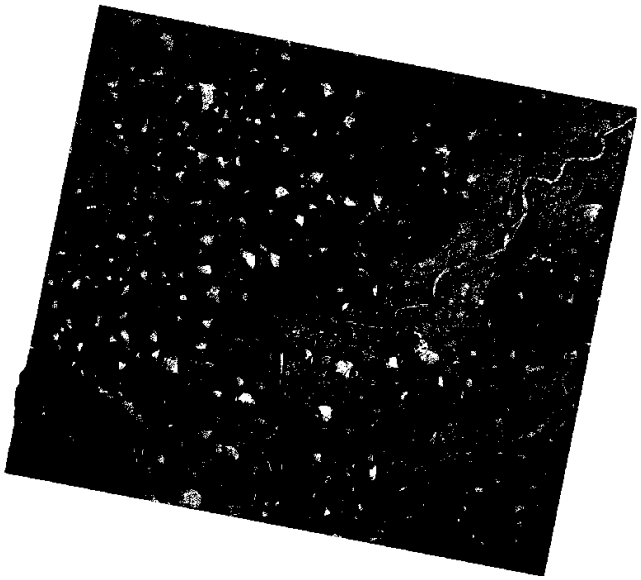

Fig 5.1 Binary flood mask

We used snap to convert the output geotif file to a kml file which can be overlapped in google earth to clearly observe the flooded regions closely and clearly. The google earth overlapped picture can be seen below. We also took the recent product with similar polygon which surrounds srikkalahasthi region and covers swarnamukhi river for comparison. As there

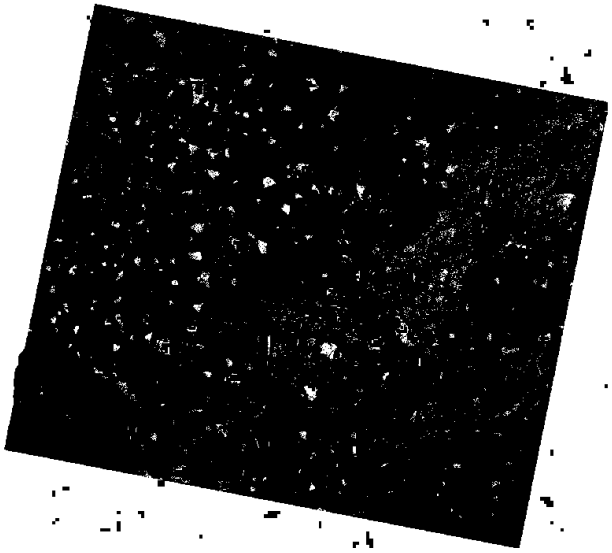

Fig 5.2 Flooded area

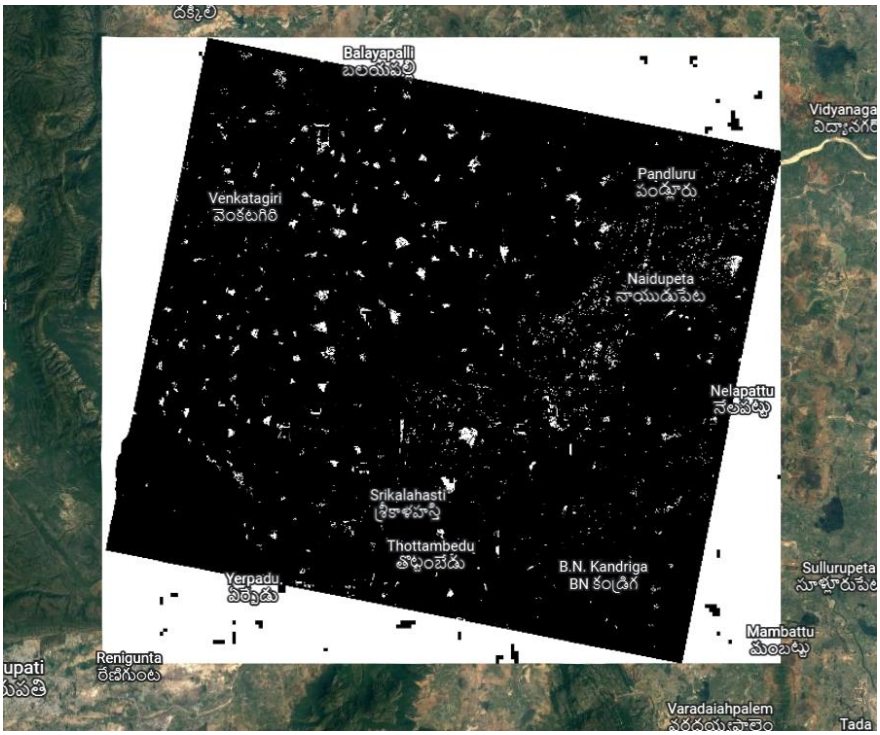

Fig 5.3 Flooded area of srikalahasti polygon during floods 2021

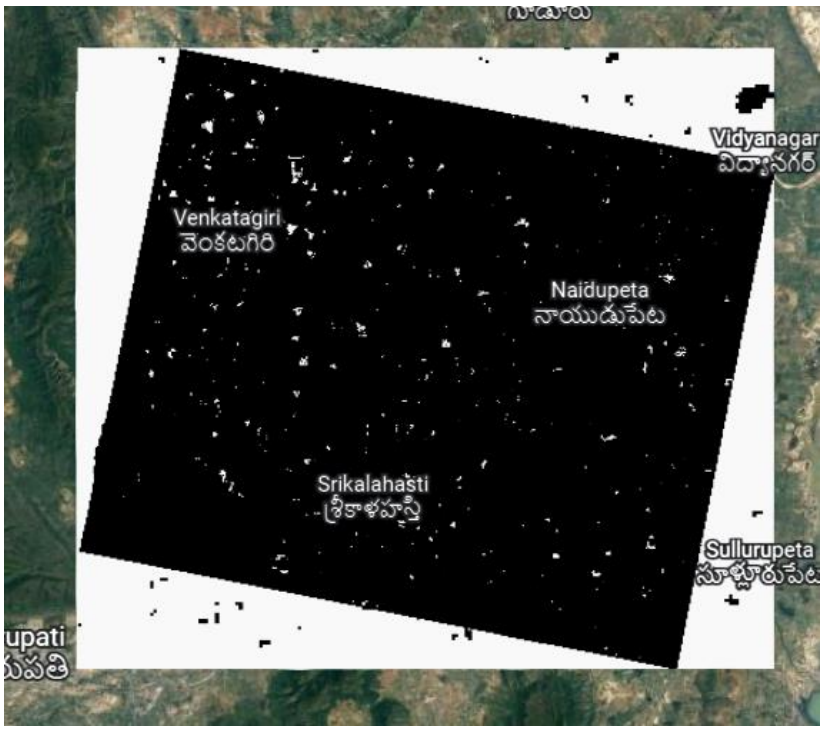

Fig 5.4 Flooded area of srikalahasti polygon recently(no floods)

are no floods recently the water in the flooded image is very low. This water might be the leakage or rain remains or extra water which is not a pond river or canal. With the following results we claim that our project is working successfully and can be useful in disaster management.

CHAPTER 6

CONCLUSION AND FUTURE SCOPE

Conclusion

Finally we conclude that it is very much useful during flood times when the water starts to enter the streets and rescue teams have to start rescue operations. This will be helpful to give an overview where water has been reached already and make a rescue plan accordingly. And it is also very much useful to study and do research in flooded region post floods for their origin and effects. A CNN machine learning program would help it further more by predicting the flood areas which can be done as extension to this project.

Future Scope

India is one of the most flood-prone countries in the world and one-eighth of the country's geographical area is subjected to floods. The flood extent mapping is critical to disaster management, humanitarian relief work and decision-making. This project can be helpful to make the disaster management robust and responsive. Even in case if the communication is lost for people to intimate for help , we can reach them out because of the monitoring we do with this project. It is much more useful for people who want to study floods and disaster management as this will give then the refined flood map of the particular area

References:

[1] Raster data: European Space Agency (ESA) - Scientific Data Hub

SRTMDEM:OpenTopo

Pythonapp:Anaconda

[2]http://gis.stackexchange.com/questions/172666/optimizing-python-gdal-readasarray

[3]http://geoexamples.blogspot.co.uk/2013/06/gdal-performance-raster-classification.html
[4]http://rintintin.colorado.edu/~wajo8931/docs/jochem_parallelsum_v2.py
[5]http://gaiamb.readthedocs.io/en/latest/_modules/gaia/gdal_functions.html
[6]http://docs.opencv.org/2.4/doc/tutorials/imgproc/threshold/threshold.html
[7]https://geohackweek.github.io/raster/02-gdal/
[8]https://books.google.com.ph/books?id=Sne9CgAAQBAJ&pg=PA153&lpg=PA153&dq=water+threshold+value+from+SAR+image&source=bl&ots=ZKGgRqub6E&sig=AMJnYJcNnlTeXwmia73ajDM8Bh8&hl=fil&sa=X&ved=0ahUKEwiJ2p-ZvsHQAhXMnZQKHZJPCZMQ6AEISDAJ#v=onepage&q=treshold&f=false
[9]https://www.ncbi.nlm.nih.gov/pmc/articles/PMC4435168/
[10]http://iopscience.iop.org/article/10.1088/1748-9326/9/3/035002
[11]http://www.itc.nl/library/papers_2016/msc/wrem/cliu.pdf
[12]http://www.isprs.org/proceedings/XXXVII/congress/6b_pdf/39.pdf
[13]https://scihub.copernicus.eu/dhus/#/home

[14]https://un-spider.org/advisory-support/recommended-practices/recommended-practice-flood-mapping/python-step-by-step

APPENDIX

```
import os

import snappy

from snappy import Product

from snappy import ProductIO

from snappy import ProductUtils

from snappy import WKTReader

from snappy import HashMap

from snappy import GPF

from snappy import jpy

# For shapefiles

import shapefile

import pygeoif


## Preprocessing functions

def applyOrbit(source):

    data = source

    params = HashMap()

    orbit =GPF.createProduct("Apply-Orbit-File", params, data)

    outfile = 'D:\\sar proj\\proj\\orbit'

    print('running orbit file')
```

```
    ProductIO.writeProduct(orbit, outfile, 'BEAM-DIMAP')
    return orbit
def subset(product,x,y,width,height):
    parameters=snappy.HashMap()
    parameters.put('copyMetadata', True)
    parameters.put('region', "%s,%s,%s,%s" %(x, y, width, height))
    subset =snappy.GPF.createProduct('Subset', parameters,product)
def calibration(product):
    parameters = HashMap()
    parameters.put('outputSigmaBand', True)
    parameters.put('sourceBands', 'Intensity_VV')
    parameters.put('selectedPolarisations', "VV")
    parameters.put('outputImageScaleInDb', False)
    print('cali done')
    return GPF.createProduct("Calibration", parameters, product)
def speckleFilter(product):
    parameters = HashMap()
    filterSizeY = '5'
    filterSizeX = '5'
    parameters.put('sourceBands', 'Sigma0_VV')
    parameters.put('filter', 'Lee')
    parameters.put('filterSizeX', filterSizeX)
    parameters.put('filterSizeY', filterSizeY)
```

```
    parameters.put('dampingFactor', '2')
    parameters.put('estimateENL', 'true')
    parameters.put('enl', '1.0')
    parameters.put('numLooksStr', '1')
    parameters.put('targetWindowSizeStr', '3x3')
    parameters.put('sigmaStr', '0.9')
    parameters.put('anSize', '50')
    print('filter done')
    sfilter=GPF.createProduct('Speckle-Filter', parameters, product)
    #ProductIO.writeProduct(sfilter, 'D:\\sar proj\\proj\\data\\filter', 'BEAM-DIMAP')
    return sfilter
def terrainCorrection(product):
    parameters = HashMap()
    parameters.put('demName', 'SRTM 3Sec')
    parameters.put('pixelSpacingInMeter', 10.0)
    parameters.put('sourceBands', 'Sigma0_VV')
    print('terrain done')
    return GPF.createProduct("Terrain-Correction", parameters, product)
# Flooding processing
def generateBinaryFlood(product):
    parameters = HashMap()
    BandDescriptor
=snappy.jpy.get_type('org.esa.snap.core.gpf.common.BandMathsOp$BandDescriptor')
```

```
    targetBand = BandDescriptor()
    targetBand.name = 'flooded'
    targetBand.type = 'uint8'
    targetBand.expression = '(Sigma0_VV < 1.13E-2) ? 1 : 0'
    targetBands  =snappy.jpy.array('org.esa.snap.core.gpf.common.BandMathsOp$BandDescriptor',
1)
    targetBands[0] = targetBand
    parameters.put('targetBands', targetBands)
    print('binary generated')
    return GPF.createProduct('BandMaths', parameters, product)
def maskKnownWater(product):
# Add land cover band
    parameters = HashMap()
    parameters.put("landCoverNames", "GlobCover")
    mask_with_land_cover = GPF.createProduct('AddLandCover', parameters,product)
    del parameters
    # Create binary water band
    BandDescriptor
=snappy.jpy.get_type('org.esa.snap.core.gpf.common.BandMathsOp$BandDescriptor')
    parameters = HashMap()
    targetBand = BandDescriptor()
    targetBand.name = 'BinaryWater'
    targetBand.type = 'uint8'
```

```
    targetBand.expression = '(land_cover_GlobCover == 210) ? 0 : 1'
    targetBands  =snappy.jpy.array('org.esa.snap.core.gpf.common.BandMathsOp$BandDescriptor',
1)
    targetBands[0] = targetBand
    parameters.put('targetBands', targetBands)
    water_mask = GPF.createProduct('BandMaths', parameters,mask_with_land_cover)
    del parameters
    parameters = HashMap()
    BandDescriptor
=snappy.jpy.get_type('org.esa.snap.core.gpf.common.BandMathsOp$BandDescriptor')
    try:
        water_mask.addBand(product.getBand("flooded"))
    except:
        pass
    targetBand = BandDescriptor()
    targetBand.name = 'Sigma0_VV_Flood_Masked'
    targetBand.type = 'uint8'
    targetBand.expression = '(BinaryWater == 1 && flooded == 1) ? 1 : 0'
    targetBands  =snappy.jpy.array('org.esa.snap.core.gpf.common.BandMathsOp$BandDescriptor',
1)
    targetBands[0] = targetBand
    parameters.put('targetBands', targetBands)
    print('masking done')
//main method
```

```
print('started')

## GPF Initialization

GPF.getDefaultInstance().getOperatorSpiRegistry().loadOperatorSpis()

path_to_sentinel_data ='D:\\sar proj\\final\\subset_0_of_S1A_IW_GRDH_1SDV_20220503T003145_20220503T003210_043039_05239E_7F46.dim'

product = ProductIO.readProduct(path_to_sentinel_data)

print('input read')

product_subset=product

product_orbitfile = applyOrbit(product_subset)

print('orbitfile done')

# Apply remainder of processing steps in a nested function call

product_preprocessed = terrainCorrection(speckleFilter(calibration(product_subset)))

bina=generateBinaryFlood(product_preprocessed)

ProductIO.writeProduct(bina, "D:\\sar proj\\final\\binary", 'BEAM-DIMAP')

product_binaryflood = maskKnownWater(bina)

ProductIO.writeProduct(product_binaryflood, "D:\\sar proj\\final\\op", 'BEAM-DIMAP')

print('finished')
```